ELSEVIER

Contents lists available at ScienceDirect

Marine Chemistry

journal homepage: www.elsevier.com/locate/marchem



Vanadium cycling in the Western Arctic Ocean is influenced by shelf-basin connectivity



Laura M. Whitmore^{a,*}, Peter L. Morton^b, Benjamin S. Twining^c, Alan M. Shiller^a

- a School of Ocean Science and Engineering, University of Southern Mississippi, 1020 Balch Blvd., Stennis Space Center, MS 39529, USA
- ^b National High Magnetic Field Laboratory, 1800 E. Paul Dirac Drive, Tallahassee, FL 32310, USA
- ^c Bigelow Laboratory for Ocean Science, 60 Bigelow Dr., East Boothbay, ME 04544, USA

ARTICLE INFO

Keywords: GEOTRACES Polar waters Vanadium Shelf dynamics Arctic Ocean

ABSTRACT

Water in the western Arctic Ocean tends to show lower dissolved vanadium concentrations than profiles observed elsewhere in the open ocean. Dissolved V in Pacific-derived basin waters was depleted by approximately 15-30% from the effective Pacific Ocean endmember. The depletion originates on western Arctic shelves and is not a result of mixing with a water mass with low V. While biological uptake may account for some of the V removal from the water column, adsorption onto particulate Fe is likely the dominant factor in removing V from shelf waters to the sediments. Once in the sediments, reduction should result in sequestering the V while Fe (and Mn) can be remobilized. A similar Fe-shuttling mechanism for V was previously described for the Peru margin (Scholz et al. 2011). Off the shelves, particulate Mn concentrations often exceed particulate Fe concentrations and thus may exert greater control on the V distribution in basin waters. Nonetheless, particulate V concentrations are much lower in basin waters and dissolved V thus behaves largely conservatively away from the shelf environment. Dissolved V concentrations in Atlantic-derived and Arctic deep waters were as much as 5 nmol/kg lower than those observed in deep waters of other ocean basins. The uniformity in deep water dissolved V between the sampled basins suggests that slow removal of V from the deep basins is probably not a factor in the deep water depletion. Vanadium-depleted incoming Atlantic waters (i.e., the source of Arctic deep waters) and/or removal of vanadium from incoming waters that pass over the shelves probably accounts for the deep water dissolved V depletion. Overall, our results demonstrate the utility of the V distribution as an additional tool to help understand the Arctic marine system. Furthermore, our work is pertinent to questions related to the net effect of marginal basin shelves on oceanic vanadium cycling, its isotopic balance, and how climateinduced changes in shelf biogeochemical cycling will impact vanadium cycling.

1. Introduction

The Arctic Ocean plays a vital role in global climate and global ocean dynamics. As Atlantic waters enter the Arctic they cool and sink, a critical process in the ocean's meridional overturning circulation. The sinking waters export materials from the surface to the ocean's interior where they can be preserved for long periods of time. Waters entering the Arctic basins are modified through shelf interactions such as sediment-water exchange, local biological uptake and remineralization, and riverine inputs. Previous research has shown that the extent and distribution of these shelf modifications may impact biogeochemical cycling (Charette et al., 2016; Fransson et al., 2001; Macdonald and Gobeil, 2012). Furthermore, the global connectivity of shelf-basin systems is currently an important study area since there is evidence that inputs from ocean margins may be large enough to account for

imbalances in oceanic elemental budgets (Charette et al., 2016; Jeandel et al., 2011). Jakobsson (2002) indicates that the shelves make up slightly more than half the area of the Arctic Ocean and this large shelf-to-basin ratio makes it an ideal region to study the role of ocean margins on basin geochemical signatures and cycling. Currently, the extent to which the shelves impart modifications on Arctic water masses, the depth of that influence, and the mechanisms driving modification remain poorly described.

There is further uncertainty regarding the influence of shelf-derived waters on Arctic deep waters partly because the processes driving geochemical signatures in Arctic deep waters are poorly understood. The Arctic Ocean basin is delineated by several topographic features. The Lomonosov Ridge divides the region into two primary basins (the Western Arctic Basin and the Eurasian Basin), both of which are further divided by other underwater ridges (Fig. 1). Bauch et al. (1995) argued

E-mail address: laura.whitmore@usm.edu (L.M. Whitmore).

^{*} Corresponding author.

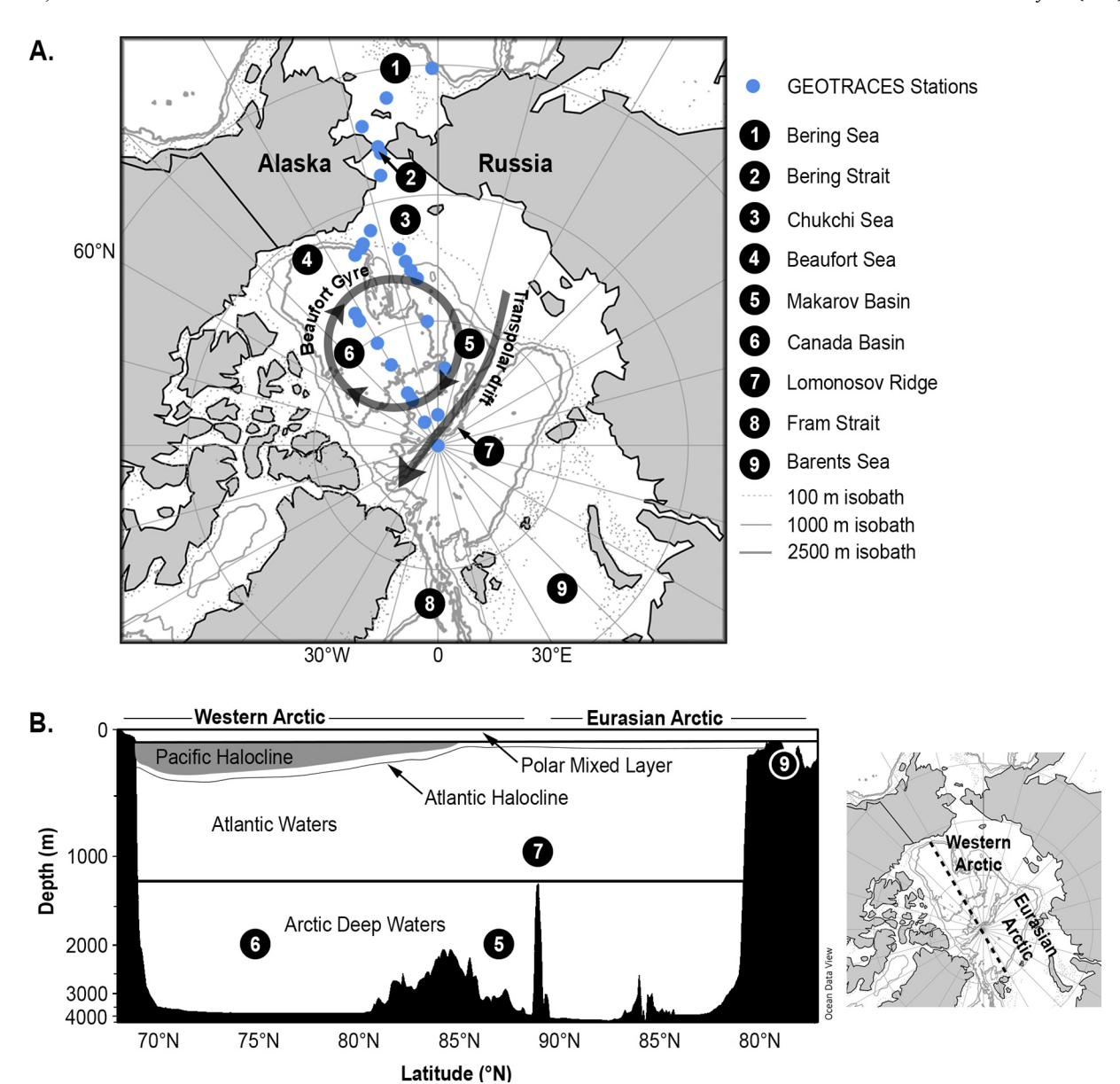


Fig. 1. Section description. (A) Map of GEOTRACES stations (blue dots) during the 2015 GN01 cruise. Numbers denote important geographic features. Gray arrows indicate major surface circulation. Dashed and solid light gray lines indicate bathymetry. (B) Cross section of the Arctic Ocean, with major water masses denoted. Geographic features are numbered as referenced in the panel A. The side map indicates the location of the cross section in the basin. (For interpretation of the references to color in this figure legend, the reader is referred to the web version of this article.)

that the different ${\rm H_2}^{18}{\rm O}$ isotopic compositions of the Western Arctic Basin and Eurasian Basin deep waters reflected differences in shelf water contributions to the basins' deep waters. Supporting the role of shelves in setting the deep water geochemistry, Roeske et al. (2012) concluded that deep water Ba concentrations were associated with Ba dissolution from shelf derived particles. Additionally, Klunder et al. (2012) indicated that the patterns in dissolved Fe in the Arctic Ocean were very basin specific and that basins with high dissolved Fe concentrations may have more resuspension at the slopes or downslope convective mixing slope interactions relative to basins with lower dissolved Fe concentrations. Further constraints are necessary to identify the relative contributions of shelf and slope processes in influencing Arctic deep water signatures.

Previous work has demonstrated that vanadium (V) cycling is linked to shelf environment and sediment processes, such as reactions associated with redox state (Beck et al., 2010; Reckhardt et al., 2017; Scholz et al., 2011; Shiller and Mao, 1999). Redox driven V removal has been observed and described (Emerson and Huested, 1991; Reckhardt et al.,

2017) but has not yet been connected to the open ocean V cycle. In pelagic environments, a slight surface water dissolved V (dV) depletion is observed (e.g., Collier, 1984; Ho et al., 2018). Shiller and Mao (1999) suggested that the open ocean surface depletion of dV might be derived from advected shelf waters with low dV concentrations.

In contrast, open ocean studies ascribe the surface dV depletion to biological uptake and export (Collier, 1984; Klein et al., 2013; Middelburg et al., 1988). Indeed, some studies have demonstrated biological uptake of V (Crans et al., 2004; Osterholz et al., 2014). Vanadium may be biologically incorporated and is associated with enzymes such as V-haloperoxidases or V-nitrogenases, although V-nitrogenases have not yet been observed in the marine environment (Crans et al., 2004 and references therein). Klein et al. (2013) concluded that biological V removal associated with diatom blooms was a significant removal mechanism for dV locally and accumulation of V by diazotrophs has been reported (Nuester et al., 2012). Additionally, V is hyperaccumulated by some ascidians, although the physiological role isn't well understood (Crans et al., 2004 and references therein).

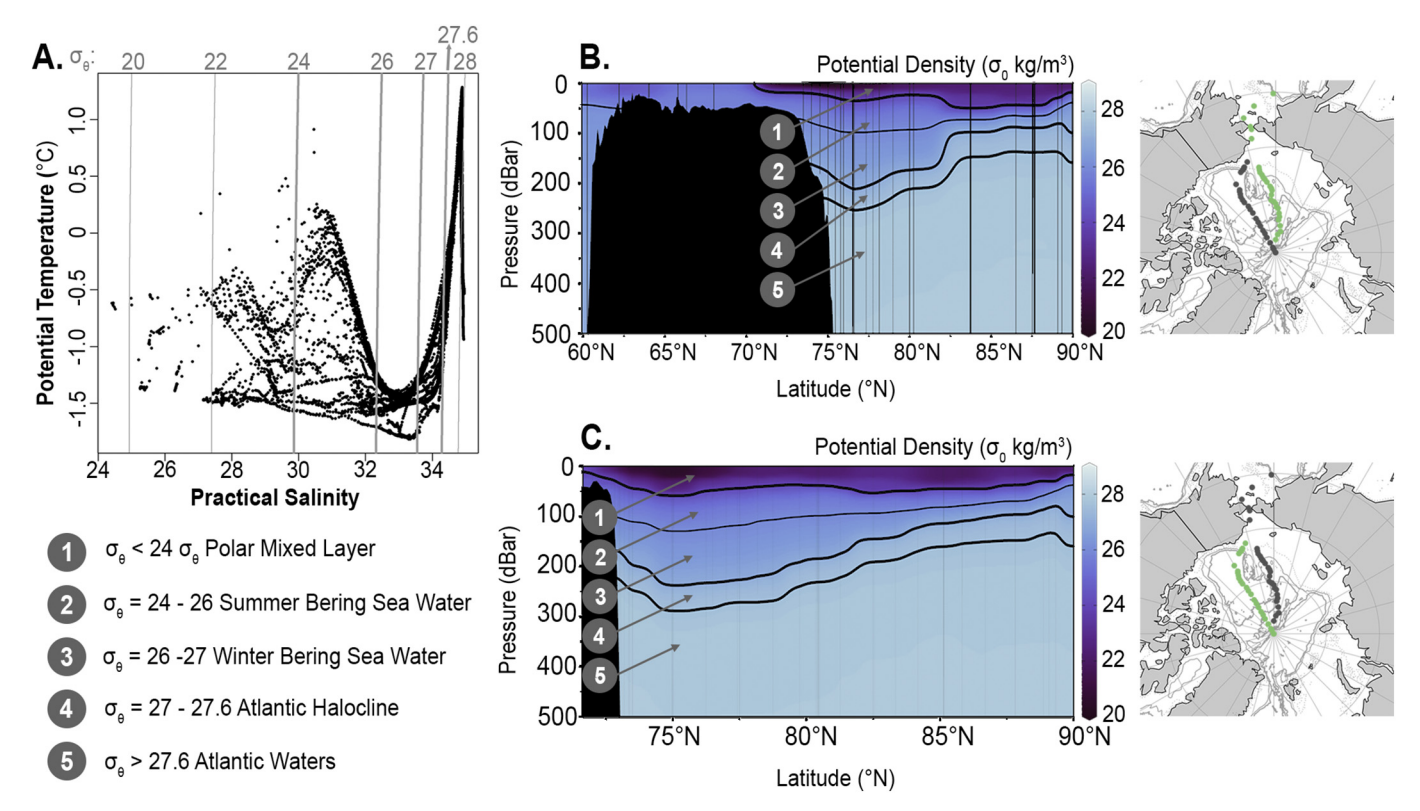


Fig. 2. Water mass descriptions. (A) Temperature-salinity plot for the GN01 Section. The gray contours represent isopycnals (σ_{θ}). Thick contour lines are the isopycnal boundaries between water masses: (1) Polar Mixed Layer < 24 σ_{θ} , (2) Pacific Halocline = 24–27 σ_{θ} , (3) Atlantic Halocline = 27–27.6 σ_{θ} , and (4) Atlantic Waters > 27.6 σ_{θ} . (B) Shelf and Makarov Basin transect for potential density with the water mass isopycnal separations denoted in contours; stations used are noted in green on the map to the right of the section plot. (C) Canada Basin transect for potential density with the water mass isopycnal separations denoted in contours; stations used are noted in green on the map to the right of the section plot. Both GEOTRACES station data and CLIVAR station data were used to generate all the figures in this panel. (For interpretation of the references to color in this figure legend, the reader is referred to the web version of this article.)

Beyond redox processes and biological uptake, in the oxic marine environment dV can be scavenged onto surfaces of particles such as iron (Fe) or manganese (Mn) oxyhydroxides (Bauer et al., 2017; Brinza et al., 2008; Koschinsky and Hein, 2003; Trefry and Metz, 1989). Particle interactions could be an important removal mechanism for dV; oxides formed in the water column sorb dV and carry it to the sediments where it may be reduced to a less soluble species (Scholz et al., 2017; Scholz et al., 2011).

Since dV has been shown to be significantly modified by shelf-associated processes (Reckhardt et al., 2017; Scholz et al., 2011; Wehrli and Stumm, 1989), basin-wide dV distributions may provide a constraint on the extent to which a water mass has been modified by the shelf. This is potentially useful for predicting nutrient stoichiometry, source chemistry, and valuable for monitoring biogeochemical changes in the Arctic Ocean due to climate change. While Shiller and Mao (1999) suggested the use of dV depletions as a tracer of shelf-derived waters, understanding the impact of this process on dV distributions in the Arctic Ocean requires better knowledge of the dV input and removal processes over the shelves and deep basins.

This study describes the first dV transect in the Arctic Ocean using samples collected during the 2015 U.S. GEOTRACES Arctic Section (GN01). This is an important step in determining the utility of dV as a tracer of shelf influences. Herein we discuss (1) the mechanisms influencing dV distribution in the basins and on the shelves, (2) the extent of shelf modification of dV, and (3) the role of shelf waters in affecting Arctic deep water composition. Our Arctic Ocean dV distributions are discussed in both local and global contexts.

2. Methods

2.1. Section introduction & geography

The 2015 US GEOTRACES Arctic Section (GN01) was conducted from August 9, 2015 to October 12, 2015 aboard the USCGC Healy. The cruise was comprised of two sections in the Western Arctic Ocean, one in the Makarov Basin and the other in the Canada Basin. The cruise was operated by U.S. GEOTRACES in conjunction with CLIVAR. Trace metal samples described in this study (i.e., dissolved V, particulate V, particulate Fe, and particulate Mn) were collected by GEOTRACES scientists at stations identified in Fig. 1; data are accessible at the Biological and Chemical Oceanography Data Management Office (BCO-DMO) database (Shiller, 2019; Twining et al., 2019). Each GEOTRACES basin station had a deep and a shallow cast that overlapped at 500 m, for a total of 23 depths. Data from the CLIVAR contingent was used to increase resolution for ancillary parameters such as nutrients, salinity and temperature (at 0.5° latitude resolution in the basins). Pigment samples were collected by the GEOTRACES contingent from shallow depths (< 100 m) at GEOTRACES stations and results were provided by cruise leadership. Ancillary data used in this study (e.g., nutrients, salinity, temperature) are located in the BCO-DMO database (Cutter et al., 2019a, 2019b).

The western Arctic Ocean is divided from the Eurasian sector by the Lomonosov Ridge. Our study was predominantly in the Western Arctic Ocean, which is further divided into the Canada and Makarov Basins by the Alpha-Mendeleev Ridge (Fig. 1). These basins have a mean depth of approximately 4000 m (Aagaard, 1981). The large shelf seas of the Arctic Ocean also influence the distribution and composition of waters in the Arctic Ocean Basins. Our study includes samples in the Bering and Chukchi Seas, but basin waters described in our study may also be

influenced by the East Siberian Sea or the Beaufort Sea.

2.2. Section hydrography

Circulation of surface waters in the western Arctic basins is influenced by atmospheric oscillations (Proshutinsky and Johnson, 1997; Steele, 2004). The Beaufort Gyre and the Transpolar Drift (TPD) are the dominant surface circulation features in the GN01 section (Fig. 1). The TPD is a major surface current that bisects the Arctic Ocean. It generally originates in the East Siberian Arctic Sea and flows across the central Arctic toward the Fram Strait. In the GN01 section, at latitudes > 85°N and depths < 50 m the presence of the Transpolar Drift (TPD) has been reported (Kipp et al., 2018).

Water column structure in the Arctic basins is complicated by transformation of seawater by brines formed when seawater freezes and by additional inputs of freshwater from rivers and sea ice melt. The presence of water types with different temperatures and salinities leads to a layering of water masses (Fig. 1B) across a large density gradient, predominantly driven by the salinity structure. In this study, water masses were defined primarily using criteria described in Steele (2004) and Talley et al. (2011), and by assessing the T-S plot of our study region with respect to previous literature (Fig. 2A).

The surface waters (the Polar Mixed Layer) of the Arctic Ocean are freshened by seasonal sea ice melt and river discharge; freezing throughout winter alters the composition of this layer via the formation of brines (Talley et al., 2011). In this study, we describe surface waters as water above the $\sigma_\theta=24\,\text{kg/m}^3$ isopycnal (i.e., above the Pacific halocline).

The Pacific halocline is comprised of waters that have entered the Arctic Ocean through the Bering Strait. Chemical properties of these waters get strongly modified by the shelf (Fransson et al., 2001; Vieira et al., 2019). The Pacific halocline is often discussed in terms of three water types, summer Bering Sea Water (sBSW), winter Bering Sea Water (wBSW), and Alaska Coastal Water (ACW) (Steele, 2004). In this study, we refer to the Pacific halocline as one unit unless otherwise indicated, meaning that where there is the presence of a warm halocline layer (sBSW or ACW) it is not discussed separately from wBSW. As such, the Pacific halocline is defined as $24 \text{ kg/m}^3 < \sigma_{\theta} < 27 \text{ kg/m}^3$. Where we discuss the influence of sBSW versus wBSW, sBSW is defined as 24 kg/ $m^3 < \sigma_\theta < 26\,\text{kg/m}^3$ and wBSW is $26\,\text{kg/m}^3 < \sigma_\theta < 27\,\text{kg/m}^3$ (Fig. 2B, C). Notably, the lateral extent of the Pacific halocline is variable and it is typically constrained to the Western Arctic basins (Alkire et al., 2015; Steele, 2004). By considering nutrient and dissolved trace element distributions, we identified the furthest extent of the Pacific halocline to be roughly at 85°N for the GN01 transect.

Directly below the Pacific halocline is the Atlantic halocline (27 km/ $m^3 < \sigma_\theta < 27.6 \, kg/m^3$). North Atlantic waters enter the Arctic Ocean via the Fram Strait (sill depth $\approx 2500 \, m$) and the Barents Sea (shelf depth $\approx 200 \, m$) (Rudels, 2019; von Appen et al., 2015). Barents Sea Branch Waters are modified and become more dense than Fram Strait Branch Waters; in the central Arctic basins, Fram Strait Branch Waters are directly below the Atlantic halocline (27.6 kg/ $m^3 < \sigma_\theta < 27.95 \, kg/m^3$) and Barents Sea Branch Waters extend from below Fram Strait Branch Waters to roughly the sill depth ($\sim 2000 \, m$) of the Lomonosov ridge (27.95 kg/m $^3 < \sigma_\theta < 28.02 \, kg/m^3$; Mauldin et al., 2010; Smethie et al., 2000).

Arctic Deep Waters are roughly defined as waters below the sill depth of the Lomonosov Ridge (Fig. 1B). The distinct formation mechanisms of Arctic Deep Water remain unclear. Studies have indicated that the chemical signature of Arctic deep waters may be representative of interactions with the shelf and slope delivered by downslope convective mixing (Bauch et al., 1995; Middag et al., 2009; Roeske et al., 2012; Rudels and Quadfasel, 1991).

2.3. Dissolved sample collection and analysis

Water column samples were collected from GO-FLO (General Oceanics) bottles on a trace metal clean rosette (Cutter et al., 2014). The surface cast collected the shallowest sample at 20 m to avoid contamination from the ship. Additional surface samples were then collected at 1 m over the edge of a small boat. Where sea ice was stable, water samples were collected at 1 m, 5 m and 20 m through a hole in the ice. Small boat and under-ice samples were collected through Teflon coated Tygon tubing using a trace metal clean pump (IWAKI, model WMD-30LFY-115). All samples were passed through pre-cleaned 0.2 µm filters (Acropak-200 or Supor; Pall Corp.) and collected into 125 mL. pre-cleaned (1.2 M HCl, rinsed with ultrapure water) high density polyethylene (HDPE) bottles; small boat and under-ice samples were first collected into large acid-washed carboys and subsampled into 125 mL bottles. Samples were acidified to 0.024 M HCl (Fisher Optima) within 1-3 months after sample collection and were stored at room temperature.

Concentrations of dV were determined using a ThermoFisher Element XR inductively coupled plasma mass spectrometer (ICP-MS) introduced with a PC3 spray chamber (Elemental Scientific). Samples were prepared for quantification using an isotope dilution method with preconcentration and matrix removal on a seaFAST system (Elemental Scientific, Inc.) following Ho et al. (2018). An enriched vanadium spike $(^{50}V = 44.3\%; Oak Ridge National Laboratories)$ was added to each sample at a volume determined from the geometric mean of the natural isotope ratio and the enriched spike isotope ratio. Approx. 14 mL of seawater sample was extracted on the seaFAST and eluted with 1 mL of 1.2 M ultrapure HNO₃. Extracted samples were introduced into the ICP- $\overline{\rm MS}$ using a ${\rm PC}^3$ spray chamber (Elemental Scientific, Inc.) to obtain the intensities of 50V and 51V. Additionally, 47Ti and 52Cr were monitored to correct for any 50Ti or 50Cr isobaric interference on 50V; the correction was generally < 1%. Reproducibility of the method was determined by assessing repeat measurements of U.S. GEOTRACES intercalibration samples (GS and GD) (Table S1); replicate measurements of GS and GD between runs had relative standard deviations of 1.8% and 1.4%, respectively (Table S1). Furthermore, GS and GD measurements were intercalibrated with those by Ho et al. (2018) and are comparable within the error of our measurements.

2.4. Particulate sample collection and analysis

Particulate samples were collected from the same trace metal clean Go-Flo bottles as the dissolved samples, by filtering an average of \sim 6 L of seawater through an acid-washed Supor polyethersulfone $0.45\,\mu m$ filter (25 mm or 47 mm) held in a Swinnex or Advantec filter holder (Twining et al., 2015). Process blanks were also generated by passing 1–2 L of filtered (0.2 μm) seawater through unused, acid-cleaned Supor filters. Sample and process blank filters were analyzed for total concentrations by digesting half of the filter in acid-cleaned PFA vials (Savillex) with 2 mL of a solution of 4 M HCl, 4 M HNO3 and 4 M HF (all Optima or double-distilled grade) and heating at 110 °C for four hours. The digest solution was transferred to a second PFA vial, to which was added 60 µL of 18.4 M H₂SO₄ (Optima) and 20 µL of 9.8 M H₂O₂ (Optima) and taken to dryness. The final residue was redissolved in 0.32 M HNO₃ (Optima or double-distilled grade) and a 10 ppb In spike added to account for matrix effects and instrumental drift during ICP-MS analysis. Full details of the method are described elsewhere (Marsay et al., 2018; Ohnemus et al., 2014; Twining et al., 2015). Labile element concentrations were determined by leaching the complementary filter half with acetic acid and hydroxylamine-hydrochloride (Berger et al., 2008), and blank corrected using leached process blank filters. Blanks and reference material recoveries are reported in Supplementary Table S2.

2.5. Data analysis

Trends between dV or pV and environmental parameters were regressed using type I or type II reduced major axis linear regression and reported with slope, correlation coefficients, and two-sided *p*-values in the supplementary material (Table S3). Shelf and basin conditions often have separate trends and are discussed separately in the text.

Averages used to describe dV of water masses in the basins were made using water column linear interpolations binned at $1\,\mathrm{m}$ intervals and averaging values between isopycnals outlined in Section 2.2 (Fig. 2). Alternatively, averages from the shelf stations were made using the discrete samples from each station.

Our discussion of particulate trace metals is divided into three primary components: (1) total particulate concentrations, (2) labile particulate concentrations, and (3) non-lithogenic particulate concentrations. Total particulate and labile particulate concentrations were determined with the methods above (Section 2.4). The lithogenic fraction was determined by applying crustal element/Al ratios (Rudnick and Gao, 2014) and calculating the lithogenic element of interest from the total pAl concentration; the assumption being made is that all pAl is lithogenic in origin. We calculate the non-lithogenic fraction by subtracting the calculated lithogenic fraction from the total particle concentration. In principle, the non-lithogenic and labile fractions determine the non-refractory component of particulate matter: biological material, readily soluble authigenic particles (e.g., oxyhydroxide phases), and/or surface-adsorbed metals (Berger et al., 2008; Ohnemus and Lam, 2015). We thus expect the non-lithogenic & labile particle concentrations to be roughly equivalent. Differences in these two fractions may arise if the global crustal ratios are not representative of our region or if the Berger leach method did not mobilize all of the nonrefractory material when particle loading is high (e.g., at shelf stations).

Section figures were made using a weighted average gridding method in Ocean Data View 5.1.5 (Schlitzer, 2018).

3. Results

3.1. Dissolved V (dV) distribution

The occupied shelf stations (stations 2-6, 66) exhibited variability in dV concentrations ranging between 26 and $32\,\mathrm{nmol/kg}$ (Fig. 3A, B). The surface waters of the Bering Sea slope station had a dV of $31.5\pm0.4\,\mathrm{nmol/kg}$ (station 1). Continental shelf stations 2 and 3, also in the Bering Sea, had dV equal to 26.1 ± 0.9 and 27.5 ± 1.5 , respectively. Despite the lower dV at stations 2 and 3, the Bering Strait station (station 4; dV = $31.4\pm0.6\,\mathrm{nmol/kg}$) had dV similar to the Bering Sea slope station (station 1) (Table 1). Stations 5 and 6 had concentrations similar to the Bering Strait station (station 4) and station 66, which was nearer the shelf break, had concentrations similar to stations 2 and 3.

In the occupied Arctic Ocean basin stations, dV had a concentration range from 13 to 22 nmol/kg in surface waters ($\sigma_\theta < 24\,\mathrm{kg/m^3}$), with the lowest concentrations in TPD-derived waters (> 85°N, < 50 m) (Stations 30–43; Fig. 3A, B); the concentrations observed in TPD-associated surface waters were roughly 10 nmol/kg less than basin surface water observations from south of 85°N. All observed surface water ($\sigma_\theta < 24\,\mathrm{kg/m^3}$) concentrations were low relative to the deep waters (29.9 \pm 1.1 nmol/kg; $\sigma_\theta > 27.9\,\mathrm{kg/m^3}$) and had a 25%–57% depletion with respect to the deep waters. Dissolved V concentrations increased with depth, and relative to surface waters, dV was slightly higher in the Pacific halocline (dV = 25.4 \pm 1.2 nmol/kg; Table 1, Fig. 3). In Atlantic and Arctic deep waters, dV is fairly constant with an average of 29.9 \pm 1.1 nmol/kg (determined using samples below the core of the Atlantic water layer: $\sigma_\theta > 27.9\,\mathrm{kg/m^3}$ for FSBW as defined by Smethie et al., 2000).

3.2. Particulate V (pV) distribution

Particulate trace metals in the Arctic have been minimally sampled and to our knowledge this is the first report of pV in the Arctic. Total pV concentrations were up to 5 orders of magnitude larger on the shelf 35-11,000 pmol/kg than in the basins (Shelf/Slope pV: (median = 370 pmol/kg);Basin pV: 4-292 pmol/kg (median = 27 pmol/kg). Shelf pV profiles generally had lower concentrations in the surface than at depth (Stations 2-6, 66; Fig. 3C, D). Dissolved V concentrations were roughly 3 orders of magnitude greater than pV concentrations. However, when comparing dV and pV distributions, one should remember that the pV concentrations represent the standing stock of suspended particulate material concentrations and not the settling flux. Thus, the magnitudes of changes in dV and pV are not directly comparable (as discussed for Cd and P cycling in Knauer and Martin, 1981), but comparison of the vertical profiles of the two phases are useful for investigating potential sources and internal transformations such as biological uptake and redox processes.

In the basins, vertical profiles of pV consistently showed a subsurface maximum, with decreasing concentrations toward the surface and at depth (Fig. 3C, D). The basin pV maximum was observed around the 26.6 kg/m³ isopycnal in a density range which encapsulated winter Bering Sea Water (wBSW) of the Pacific halocline and the Atlantic halocline ($\sigma_\theta \approx 26\text{--}27.3\,\text{kg/m}^3$). Additionally, elevated pV concentrations were observed along the continental slopes with the highest concentrations on the shelves. The spatial trends observed between the non-lithogenic, labile, and total pV were similar (Fig. S1).

The non-lithogenic fraction of pV represented 47%-83% (median = 63%) of the total pV on the shelves and 43%-100% (median = 80%) in the basins. The labile fraction of pV represented 15%-100% (median = 36%) of total pV on the shelves and 5% - 100% (median = 64%) in the basins. Such a large labile pool indicates a substantial amount of the pV distribution is associated with in situ formation of pV and/or represents a form of pV that may be bioavailable.

4. Discussion

4.1. Comparison of Arctic dV distribution to other ocean basins

Outside of the Arctic Ocean, typical oceanic profiles of dV are slightly depleted at the surface and increase with depth to a concentration of 32.5–35 nmol/kg. Surface dV is usually depleted by approximately 10% relative to deep waters, although some observations indicate more substantial surface depletions attributed to biological activity (Collier, 1984; Ho et al., 2018; Klein et al., 2013). The surface depletion we observed in the Western Arctic Ocean was 25–57%. The deep water ($\sigma_\theta > 27.87 \, \text{kg/m}^3$) dV in the Western Arctic Ocean basins (29.9 \pm 1.1 nmol/kg) is up to 5 nmol/kg lower than previous observations in the Pacific and North Atlantic Oceans (i.e., Collier, 1984; Ho et al., 2018; Klein et al., 2013; Middelburg et al., 1988; Fig. 4).

The differences in dV distribution compared to the Pacific and Atlantic Oceans may stem from the unique features of the Arctic Ocean, including high riverine input and shelf exposure relative to basin area. Herein, we suggest that the dV structure in the Arctic basins reflects the source water type and the extent to which that water has been modified on the shelf.

4.2. The Pacific halocline & surface waters

All water entering the Arctic from the Pacific is channeled through the Bering Strait. This concentration is our effective Pacific endmember (dV = 31.4 \pm 0.6 nmol/kg; Station 4, Table 1). However, between the Bering Strait and the basins there was a significant decrease in dV (Fig. 3A, B). By comparing dV in the Bering Strait endmember to dV in the Pacific halocline (i.e. along the same isopycnal range, σ

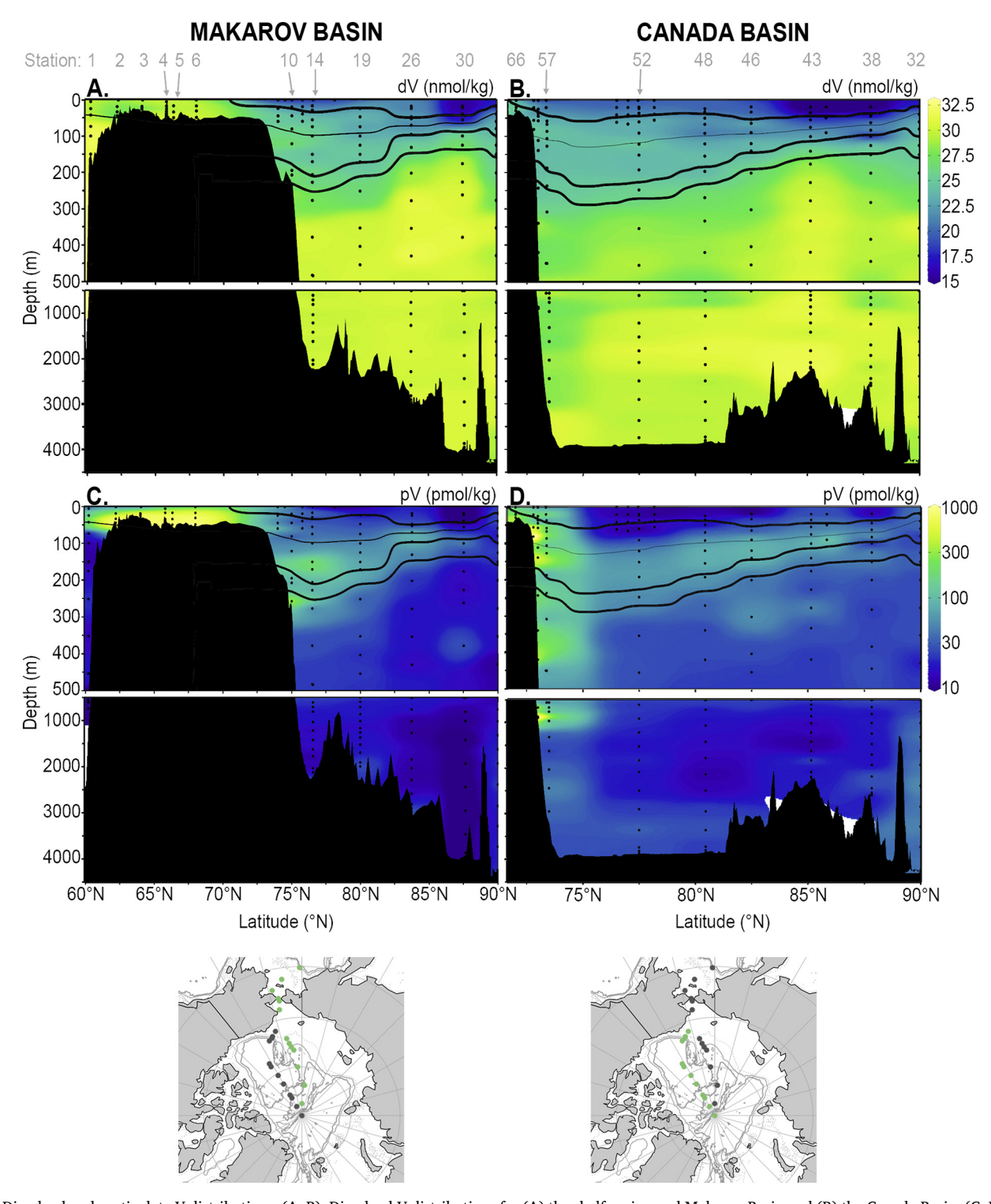


Fig. 3. Dissolved and particulate V distributions. (A, B): Dissolved V distributions for (A) the shelf region and Makarov Basin and (B) the Canada Basin. (C, D): Total particulate V distributions for (C) the shelf region and Makarov Basin and (D) the Canada Basin (the color scale is logarithmic). The location of the transect is indicated in green on the maps below the sections and station numbers are indicated above the sections. The contours are isopycnals delineating water masses as described in Fig. 2. In panels A & C, caution should be used interpreting the gradient between Station 6 and 10, as there are few data points to inform the gridding. (For interpretation of the references to color in this figure legend, the reader is referred to the web version of this article.)

 $_{\theta}$ = 24–27 kg/m³), we observed a 5–9 nmol/kg decrease in dV, or 17–30% removal of dV between the effective Pacific endmember and Pacific halocline waters (ΔV).

Additionally, an extremely low near surface dV signal north of $85^{\circ}N$ (Stations 30–43; Fig. 3A, B) provides further evidence for shelf influence on the dV distribution in the basins (dV = 11.9-21.6 nmol/kg).

The surface waters north of 85°N are associated with the TPD, which has been demonstrated to carry a significant shelf-derived radium signal ($\leq 50 \text{ m}$; Kipp et al., 2018). In addition to the shelf-derived radium signal, a higher fraction of river water ($\sim 20\%$) was also reported in the TPD waters (Kipp et al., 2018).

There are four plausible mechanisms that may drive the observed

Table 1
Mean dV concentrations of several water types discussed in the text.

Region	Station	dV (nmol/kg)		
		Mean	SD	n
Bering Sea Slope, surface	1	31.5	0.4	4
Shelf (Bering Sea)	2	26.1	0.9	4
Shelf (Bering Sea)	3	27.5	1.5	4
Shelf (Bering Strait) ^a	4	31.4	0.6	4
Shelf (Chukchi Sea)	5	30.7	1.0	3
Shelf (Chukchi Sea)	6	30.4	0.5	4
Shelf (Beaufort Sea)	66	26.0	0.6	4
Pacific Halocline ^b	10-30, 48-60	25.4	1.2	11
Atlantic/Deep Arctic Waters	14-57	29.9	1.1	161

^a Bering Strait Endmember (effective Pacific Endmember).

^b An average of each station's Pacific halocline mean, determined using interpolated profiles.

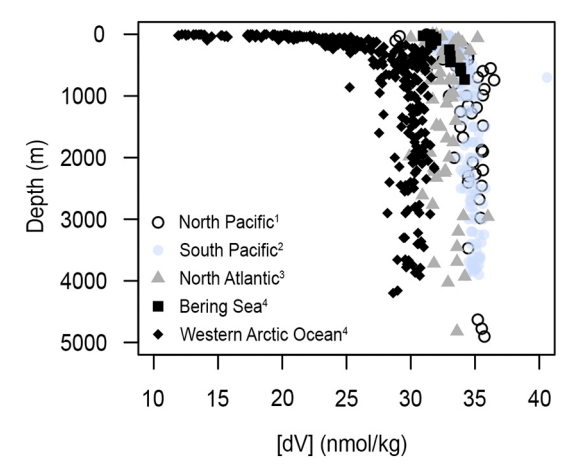


Fig. 4. Global comparison of dV profiles. Comparison of Arctic dV data (this study) to previously published Pacific and Atlantic V data: (1) Collier, 1984; (2) Ho et al., 2018; (3) Middelburg et al., 1988; (4) This study.

low dV signals in the basin which will be assessed in the following sections: (1) mixing with low dV water types (i.e., dilution; section 4.2.1), (2) dV removal associated with biological activity (Section 4.2.2), (3) inorganic particle scavenging of dV (Section 4.2.3), and (4) influences of reducing shelf sediments (Section 4.2.4).

4.2.1. Influence of water-type mixing on dV distribution

Conservative mixing of different water types can influence the distribution of dV. In this section we aim to separate potential dV depletion due to mixing of lower dV waters from depletion due to nonconservative processes. In the Arctic basin there are several water types with different endmember dV concentrations including sea ice melt, riverine input, Pacific-derived waters, and Atlantic-derived waters. Both sea ice melt and riverine inputs are characterized by low salinity and low dV relative to the Pacific-derived or Atlantic-derived seawater (Marsay et al., 2018; Peterson et al., 2016).

Given the strong covariance between salinity and dissolved V (dV; Fig. 5), we took a two-pronged approach to assess the relative contribution of these low salinity endmembers to the observed dV distributions. Both approaches utilize a two endmember mixing model (Eqs. (1)–(3)), where f indicates the fraction of freshwater or saline water, [dV] indicates the concentration of dissolved V, and S indicates salinity in the observed fresh or saline endmembers.

$$1 = f_{fresh} + f_{saline} \tag{1}$$

$$[dV]_{obs} = [dV]_{fresh} \cdot f_{fresh} + [dV]_{saline} \cdot f_{saline}$$
(2)

$$[S]_{obs} = [S]_{fresh} \cdot f_{fresh} + [S]_{saline} \cdot f_{saline}$$
(3)

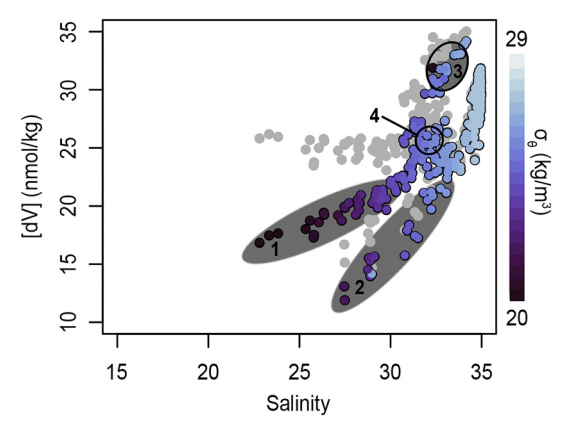


Fig. 5. Dissolved V versus salinity. All samples were used in plotting this figure. Original data ($\mathrm{dV}_{\mathrm{obs}}$) are filled with the density color bar and outlined in black and salinity normalized data ($\mathrm{dV}_{\mathrm{saline}}$) are gray circles. The circled regions and numbered regions indicate: (1) Surface waters south of 85°N, (2) Surface waters north of 85°N (i.e., TPD-influenced), (3) Bering Sea and Strait (i.e., roughly the Bering Sea endmember), and (4) The Pacific halocline. The largest correction between the observed and the normalized (group 1) contains surface waters south of 85°N (i.e., group 1) where many samples are influenced by sea ice melt in the marginal ice zone.

The first approach is a salinity normalization, which assumes that the freshwater fraction has $[S]_{fresh} = 0$ and $[dV]_{fresh} = 0$. In doing this, we can rearrange the equation to solve for $[dV]_{saline}$ (Eq. (4)). We consider these assumptions reasonable because the main sources of freshwater to the Arctic Ocean (sea ice melt and river discharge) have low concentrations of dV (Marsay et al., 2018; Peterson et al., 2016).

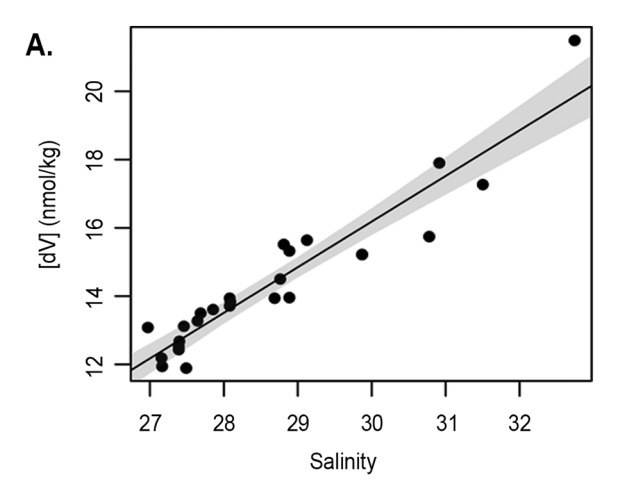
We account for the influence of conservative mixing by normalizing our observed data (dV_{obs}, S_{obs}) to a reference salinity (S_{saline}) of 35 (Eq. (4); Fig. 5). We recognize that this is higher than Pacific seawater (S \approx 32.5) and slightly higher than Atlantic waters (S \approx 34.9), so all samples will have a slight positive offset.

$$[dV]_{\text{saline}} = \frac{[dV]_{\text{obs}}}{S_{\text{obs}}} \times S_{\text{saline}}$$
(4)

In this approach, salinity-normalized dissolved V (dV_{saline}) preserves non-conservative changes in dV while removing the influence of conservative mixing with low dV, low salinity endmembers such as ice melt or river discharge. Stations that were within the marginal ice zone – the transitional zone between open ocean and sea ice covered seas – had surface samples that were significantly influenced by dilution (Stations 8–14 and 51–54; Figs. 3 and 5). This result is expected as the dV in ice samples collected during the GN01 cruise was 0.3–4.4 nM (Marsay et al., 2018).

We reevaluate the change in V (ΔV) between the Bering Sea endmember and the Pacific-halocline using the salinity normalized dV by subtracting the average dV_{saline} of the Pacific halocline at each station from the average dV_{saline} from the Bering Strait; this resulting nonconservative ΔV (ΔV_{saline}) yielded a difference of 5–10 nmol/kg, equivalent to a 17%–33% removal of dV. This range is the same as the ΔV derived from the un-normalized data, indicating that conservative mixing of our Pacific endmember with a low-salinity, low-dV water mass does not account for the depletion of dV in the Pacific halocline relative to the Bering Strait inflow. Thus, an additional mechanism(s) is required to account for the observed ΔV .

Our second approach uses data from TPD-influenced waters in the central Arctic. In these waters, we had a range of salinities from 27 to 33. We made no initial assumption on what the fresh dV endmember would be and instead used the dV and salinity data to inform our endmember. In plotting dV versus salinity along this section, a strong linear correlation is apparent ($r^2 = 0.89$; p < .001; (Fig. 6A). Using this correlation, we extrapolated back to the zero-salinity endmember



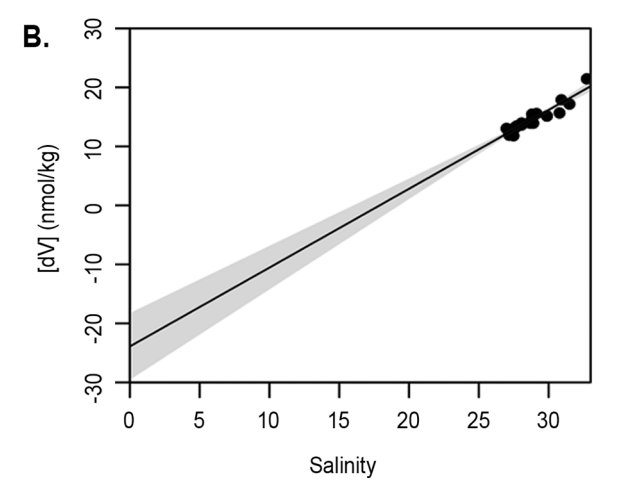


Fig. 6. TPD dV versus salinity. (A) Type I least squares regression for observed TPD dV data. (B) Regression extrapolated to the zero-salinity endmember. The gray band in both panels represents the 95% confidence interval. Negative dV at the zero salinity endmember indicates there must be dV removal processes between the river source and the basin.

and determined the apparent endmember dV_{fresh} to be approximately $-24\,\mathrm{nmol/kg}$ (Fig. 6B, see figure for 95% confidence interval). The negative result implies significant removal in the estuarine and/or shelf environment.

The effect of dilution from low-salinity, low-dV endmembers such as river water or sea ice melt therefore does not account for the ΔV observed in the Pacific halocline or the low dV waters in the TPD. With that in mind, we investigated other potential removal mechanisms,

including biological removal, dissolved-particulate interactions, and redox reactivity, discussed in detail in the following sections.

4.2.2. Biological removal of dV

It has been proposed that the surface ocean depletion of dV is, to some degree, the result of biological uptake (e.g., Collier, 1984; Middelburg et al., 1988). This biological uptake may be unintentional due to the chemical similarity of vanadate and phosphate. However, a direct biological need for V has also been demonstrated in marine systems. For example, V is utilized in V-haloperoxidases (Crans et al., 2004), which are found in a variety of organisms including some diatoms. This might explain the observations of Klein et al. (2013) and Osterholz et al. (2014) who demonstrated scavenging removal of V associated with diatoms. Elevated V in North Atlantic Trichodesmium supports a role for V in diazotrophs (Nuester et al., 2012), though V nitrogenases have so far only been identified in soil organisms. Interestingly, recent studies have demonstrated N2-fixation is occurring Arctic-wide (Blais et al., 2012; Fernández-Méndez et al., 2016; Harding et al., 2018; Sipler et al., 2017); thus, V uptake by diazotrophs may facilitate removal of dV in the Arctic water column. To evaluate whether biological processes might significantly influence the V cycle in the Arctic, we used several approaches comparing our dV and pV data with ancillary pigment and nutrient data.

To investigate the relationships with biological activity, we first compared dV and pV to total chlorophyll-a and to fucoxanthin (an accessory pigment found in diatoms) (Fig. 7, Fig. S2). We found weak correlations for dV or log-transformed pV and log-transformed pigments (i.e., chlorophyll-a or fucoxanthin; $r^2 < 0.5$ for any tested combination of pigments and dV or pV; Table S3). Significant p-values were determined in consideration of all data or shelf-only regressions; basin-only regressions had insignificant p-values (Table S3). In a system with substantial biological control, we expect pV and pigments to trend positively and dV and pigments to trend negatively. Our observations indicate a generally positive trend between pV and pigments, as expected (Fig. 7B); however, we also observed a positive trend between dV and pigments which is opposite of the expectation (Fig. 7A, Table S3). This suggests that while there may be an association between biological activity and V, it does not drive the dV distribution.

Similarly, linear relationships between dV or pV and dissolved nutrients were not observed in this study (Fig. S3). This may be due to the preferential regeneration of nutrients in shelf sediments relative to V: vanadium delivered to the sediments (by particle scavenging or biological uptake and settling) is potentially retained under reducing conditions commonly found in sediments (e.g., Breit and Wanty, 1991; see Section 4.2.4), whereas nutrients may diffuse back into the water column during remineralization. Cid et al. (2012) compared bioactive trace element and major nutrient relationships in the Chukchi and Beaufort Seas and concluded that trace metal distributions (excepting

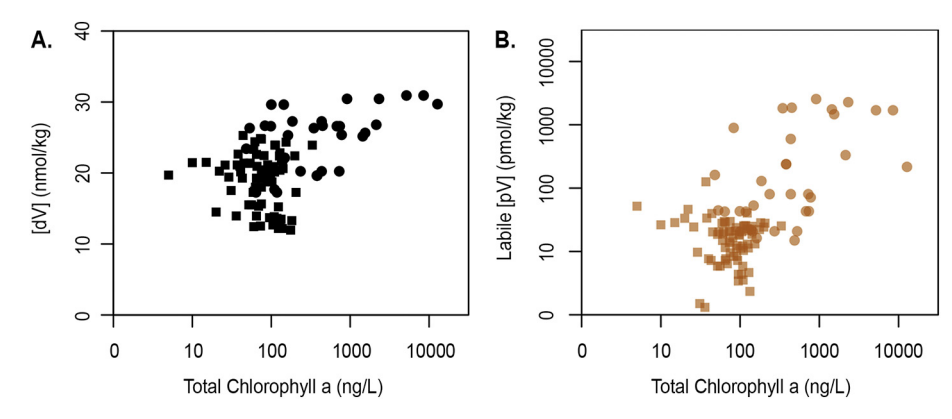


Fig. 7. Dissolved and particulate V versus total chlorophyll a. (A) Dissolved V concentration plotted against total chlorophyll a. (B) Labile pV versus total chlorophyll a. Circles indicate data from shelf stations and squares indicate data from basin stations.

Table 2 Summary of literature particulate V:P, V:Fe, and V:Mn ratios (in mmol:mol).

Publication	V:P	V:Fe	V:Mn
Ohnemus et al., 2017 ^c	0.17-4.6	4.15	_
Ho et al., 2018 ^c	4	5.3	_
Osterholz et al., 2014	10	_	_
Nuester et al., 2012	41-63	_	_
Bauer et al., 2017	-	_	0.3
Klein et al., 2013	0.076-0.38	_	_
Tang & Morel, 2006	0.018-0.020	_	_
Tovar-Sanchez & Sañudo-Wilhelmy, 2011	5-11.4	_	_
Feely et al., 1998	_	2.3-4.4	_
Our Study (labile, nonlithogenic)	-	^a 3.6, 7.6	^b 8.8, 12.5

- a Shelf-only data.
- Basin-only data.
- ^c V:P and V:Fe were determined using subsets of large oceanic sections. V:Fe was determined using hydrothermally-impacted waters with the assumption that all particulate Fe was derived from the oxidation of hydrothermal Fe. In contrast, V:P ratios were assessed after correction for lithogenic and Fe-oxide contributions in waters expected to have a dominant biological profile, such as the surface mixed layer.

Cd) were not dominated by biological uptake and remineralization. While V was not included in their study, the dV-nutrient relationships from our Arctic samples are consistent with the conclusions of Cid et al. (2012).

Relationships between dissolved V and nutrients may not be representative of biological uptake ratios. To account for this, we utilized a biological ratio of V:P estimated from the literature and our labile particulate phosphorus (pP) concentrations to predict the biological pV (pV_{BIO}) signal: $pV_{BIO} = V/P * pP_{Labile}$, where V/P is the molar ratio of these elements in biological materials. Our approach assumes all the observed labile pP was biological in origin. Published particulate V:P ratios range from 0.018-63 mmol:mol (Table 2). We applied a V:P ratio of 0.5 mmol:mol, which is roughly the median of the range reported for the mixed layer in the Equatorial Pacific (0.17-2.6 mmol:mol; Ohnemus et al., 2017) and slightly higher than the range of values reported by Klein et al. (2013) for surface waters of the North Atlantic (0.076–0.38 mmol:mol: Table 2). Higher literature estimates are usually condition-specific (e.g., in an oxygen deficient zone: Ho et al., 2018; Ohnemus et al., 2017). The highest literature V:P estimates are from Trichodesmium in P-limited conditions in the North Atlantic (63 mmol:mol; Nuester et al., 2012) or under stationary phase conditions in isolated culture samples (10 mmol:mol; Osterholz et al., 2014). These two situations are unlikely to be representative of either the bulk Arctic planktonic community or the P-replete conditions of the western Arctic Ocean and thus we discount them as appropriate estimates.

The resulting distribution of pV_{BIO} suggests that pV_{BIO} can only account for a substantial fraction of labile pV in surface waters, $<50\,\mathrm{m}$ depth in the basin and $<15\,\mathrm{m}$ over the shelves (Fig. 8C, D). A few samples over-predict pV_{BIO} (i.e. pV_{BIO} > labile pV), which indicates that our estimate of biological V:P may be an overestimate at some stations (i.e., surface waters at the Bering Sea Slope – station 1, on the shelf – station 3, and in the marginal ice zone – station 14). Furthermore, we note that the relationship between labile pV and labile pP, while positive, is not strongly correlated on the shelf or in the basin (r² <0.2; p>.09) (Fig. 9A, B). In this comparison, we again assumed that all of the observed labile pP was biogenic. We interpret the weak correlation as evidence that the observed pV signal is not strongly driven by biological uptake.

Our investigation of various biological proxies and dV and pV distributions suggest that V removal by biological uptake is not the dominant mechanism of dV removal in the Western Arctic Ocean. In our results (Section 3.1), we noted that stations 2, 3, and 66 had lower dV concentrations than other shelf stations (Table 1); we postulate that this may be due to a stripping of dV in the surface resulting from bloom

conditions or resuspension of sediments. Particle profiles at these stations have low particle concentrations in the surface and high particle concentrations at depth (Fig. S4). This profile shape may be indicative of post-bloom conditions at stations 2 and 3 and/or resuspension at the seafloor.

We conclude that while biological uptake may contribute to the removal of dV in near surface waters, it does not appear to have a large influence below the surface water layer; therefore, biological uptake cannot explain the observed depletion in the Pacific halocline of 8–9 nmol/kg (Δ V). Notably, this assessment would be improved by further constraints on cellular V:P ratios.

4.2.3. Chemically-driven particle interactions

Generally speaking, Arctic basins have low particle concentrations, including both POC and particulate trace elements, compared to other ocean basins (Honjo et al., 2010; O'Brien et al., 2013). Nonetheless, lateral transport of particulate trace metals from the shelf into the basin has been described for some trace metals (Aguilar-Islas et al., 2013; Kondo et al., 2016; Macdonald and Gobeil, 2012).

We can hypothesize that pV distributions in the Arctic Ocean would be similar to pFe or pMn due to scavenging of dV onto oxyhydroxide surfaces. We suspect that particle scavenging may lead to a substantial sink of dV when coupled with reducing sediment conditions whereby V may be further immobilized (Scholz et al., 2011, 2017). Under oxic conditions, dV species predominantly exist in the V(V) oxidation state, although small amounts of V(IV) may be stabilized by organic complexes (Huang et al., 2015 and references therein). While V(V) has not been demonstrated to be strongly complexed with organics in the marine environment, various studies have demonstrated scavenging of V(V) by ligand exchange onto Fe and Mn oxyhydroxides (e.g., Bauer et al., 2017; Brinza et al., 2008; Wehrli and Stumm, 1989). The dominant association of V is likely to depend on the relative concentrations of pFe and pMn (as suggested in Bauer et al., 2017). Partition coefficients can be of a similar order of magnitude for Fe and Mn oxyhydroxides, roughly 2000 to 90,000 L kg⁻¹ for Fe oxyhydroxides and ~60,000 L kg⁻¹ for Mn oxyhydroxides (Huang et al., 2015 and references therein; Takematsu et al., 1985) Similarly, Scholz et al. (2017) described Mn as a dominant scavenger in the surface ocean above the oxygen minimum zone, but Fe oxides predominated within the oxygen minimum zone. In our section, pFe is higher on the shelves than pMn, and thus pFe likely has more control on V cycling than pMn. However, in the basins pMn is often greater than pFe and, thus, pMn may have a greater relative influence on V cycling in the basins than it does on the shelves. That said, because pFe is much greater on the shelves than either pFe or pMn in the basins, scavenging of V onto oxyhydroxide surfaces is likely far more important on the shelves than in basin waters.

To test the influence of authigenic marine oxides on pV (designated as "pV_{CHEM}"), we determine the component of labile pV due to Fe oxides (pV_{CHEM}, $_{\rm Fe}$) and Mn oxides (pV_{CHEM}, $_{\rm Mn}$) by utilizing particulate V:Fe and V:Mn ratios from the literature (Eqs. (5), (6))

$$pV_{CHEM,Fe} = \frac{V}{Fe} \times pFe_{Labile} \tag{5}$$

$$pV_{CHEM,Mn} = \frac{V}{Mn} \times pMn_{Labile} \tag{6}$$

We applied the V:Fe ratio reported in Ohnemus et al. (2017) (Table 2), which was determined by assessing hydrothermal plume samples and assuming all the pFe was sourced from oxides formed when hydrothermal waters entered the oxic marine environment. Other studies have also assessed the V:Fe ratio in hydrothermal plume-associated samples (Table 2; Ho et al., 2018; Feely, 1998) and reported V:Fe ratios similar to Ohnemus et al. (2017). Both Ho et al. (2018) and Ohnemus et al. (2017) discuss possible limitations of applying a hydrothermal V:Fe ratio specifically to particle interactions elsewhere. However, upper water column V:Fe ratios specific to the Arctic shelf Fe-

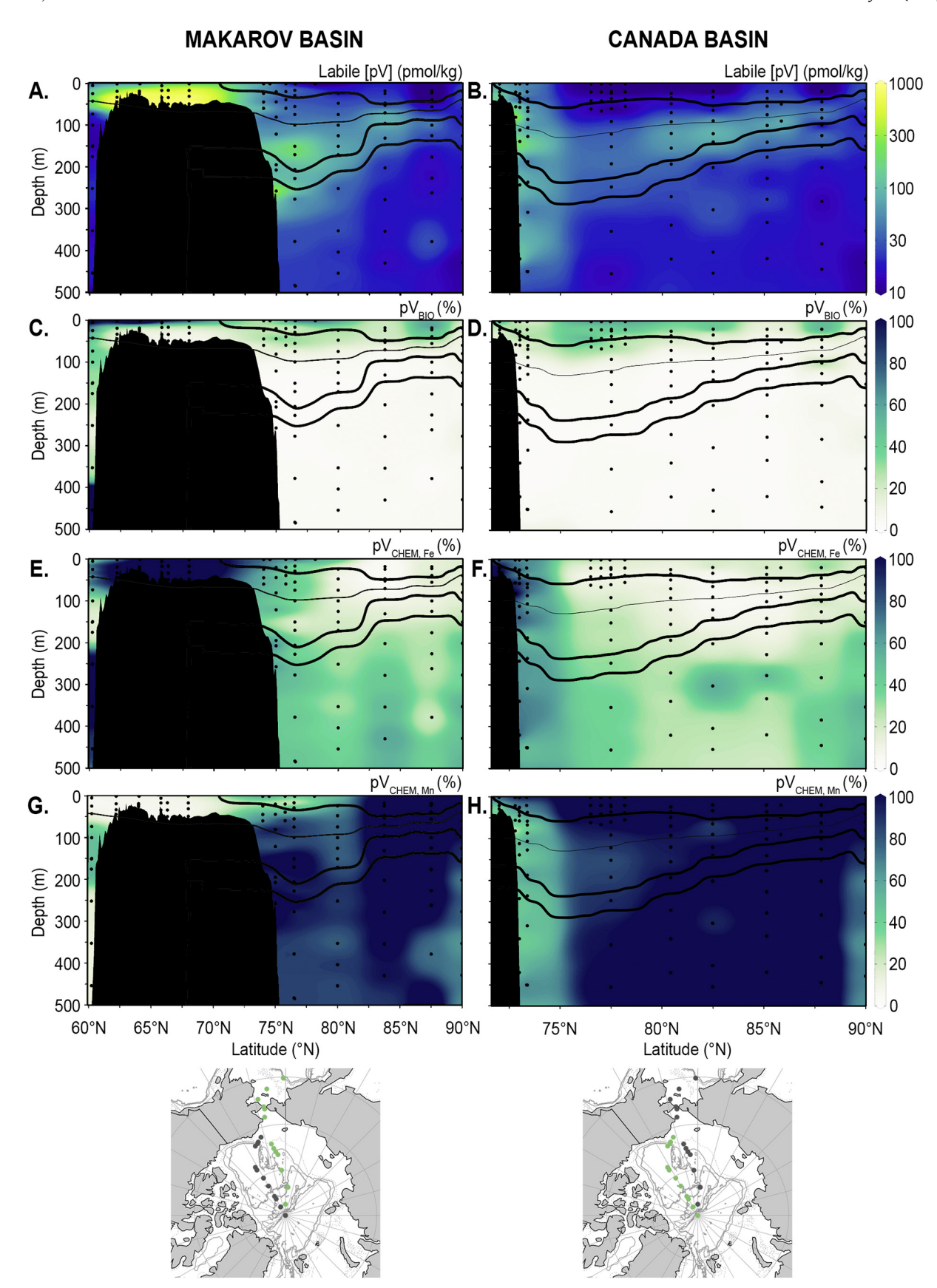


Fig. 8. Process associated labile pV distributions. (A, B) The distribution of labile pV in the surface 500 m (the color scale is logarithmic). The relative amounts of labile pV (%) that are associated with (C, D) biological particles, (E, F) iron oxide-derived particles, and (G, H) manganese oxide-derived particles. The Makarov and Canada Basin sections are the left panel and right panel, respectively; the color bar for the z variable is located to the far right of each pair and the section location can be identified in the maps at the base of the figure. The contours on each panel are isopycnals delineating water masses as described in Fig. 2. Full depth section profiles are provided in the supplementary material (Fig. S5a, b).

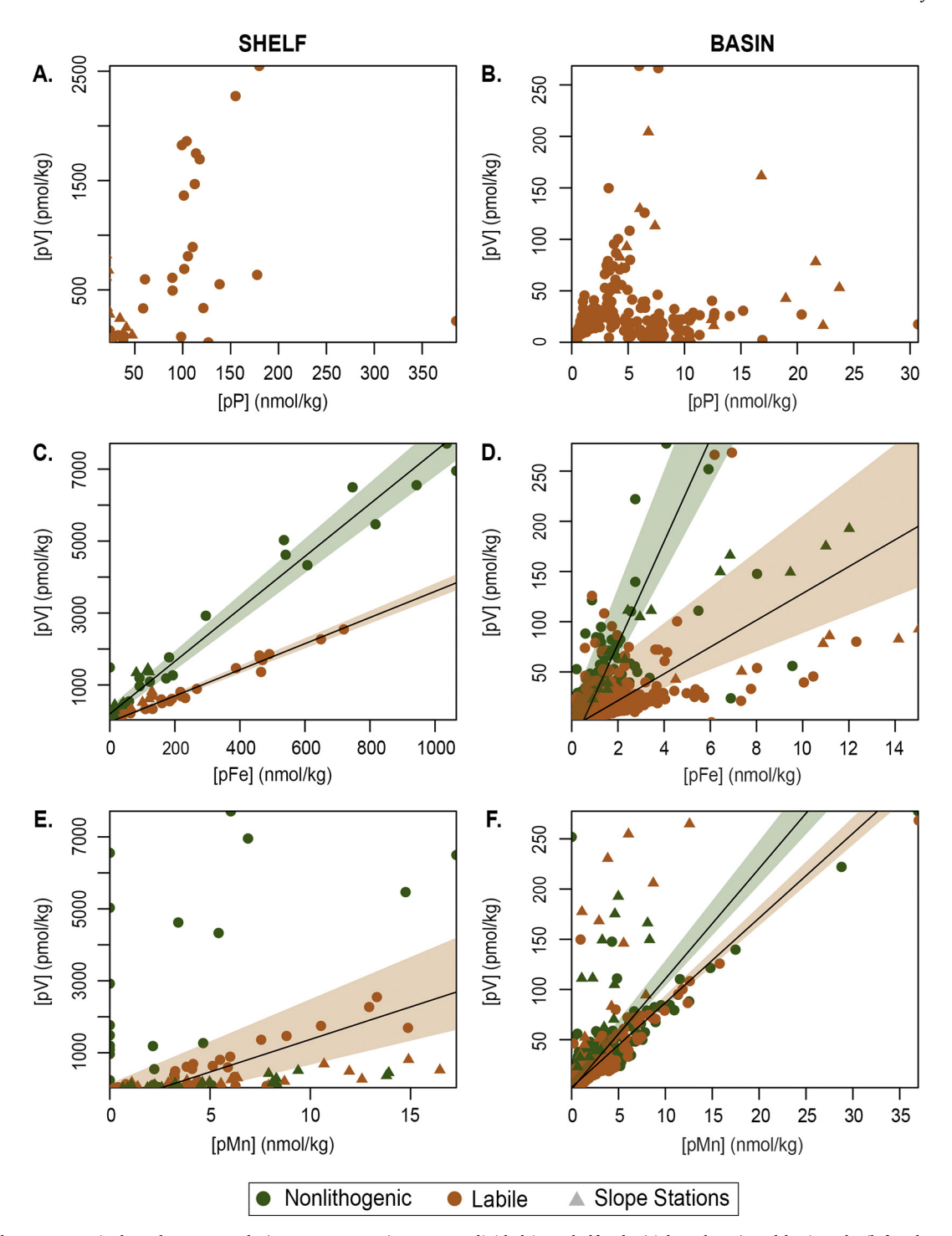


Fig. 9. Particulate V to particulate-element trends (pP, pFe, or pMn). Data are divided into shelf-only (right column) and basin-only (left column) scatter plots. Because of large regional differences in particle abundance, axis ranges between the shelf and basin panels are variable. Slope data are plotted on both shelf-only and basin-only plots and marked with triangles. A,B) The pV:pP relationship, which is positive but not strongly correlated. C,D) The pV:pFe relationship, which is strongly correlated (see Table S3 in the supplemental for more statistical information). E,F) The pV:pMn trend: basin-only data and the labile shelf data yield significant relationships. In all panels, dashed lines indicate the trendline of a type II major axis linear regression, while the colored bands indicate the 95% confidence interval determined from a jackknife procedure (n = 1000).

oxyhydroxide phase have not been described, therefore application of V:Fe ratios from hydrothermal systems is our most reasonable option.

The estimated pV_{CHEM, Fe} accounts for all of the observed labile pV over the shelves (Fig. 8E, F). In contrast to the shelf region, the labile pV in the basins cannot be entirely accounted for by pV_{CHEM, Fe} (Fig. 8E, F). Notably, pV_{CHEM, Fe} exceeded 100% of the measured labile pV in 13% of water column samples; of the samples exceeding 100%, a range from

 $102\%{-}165\%$ was observed – the majority of which are located on the continental shelf. Considering pV_{CHEM, Fe} determined from non-lithogenic pFe, roughly 60–70% of non-lithogenic pV can be accounted for using the V:Fe relationship. In the case of non-lithogenic pV_{CHEM, Fe}, only one water column sample exceeded 100% of the observed non-lithogenic pV, this sample was at 1 m and collected directly under the sea ice; it was >100% for the labile fraction as well.

The difference in non-lithogenic and labile pV_{CHEM}, $_{Fe}$ may be attributed to methodological concerns mentioned in section 2.5. Even though the fraction of pV that non-lithogenic pV_{CHEM}, $_{Fe}$ accounts for is less than observed for labile data, the distribution of pV_{CHEM}, $_{Fe}$ determined from non-lithogenic pFe has the same distribution of as pV_{CHEM}, $_{Fe}$ determined using labile pFe. Thus, for our purposes in assessing the relative role of Fe-oxide interactions on dV, either result is appropriate.

We further examined the relationship between pV and pFe using non-lithogenic and labile fractions in property-property space. Both non-lithogenic and labile pV and pFe exhibit tight positive correlations in the shelf regions ($r_{\rm nonlithogenic}^2 = 0.96$, p < .001; $r_{\rm labile}^2 = 0.98$, p < .001; Fig. 9C). The slopes of these relationships are 7.3 and 3.6 for the non-lithogenic and labile fractions, respectively. This is a broader range than reported in other studies, but encompasses the ratios presented in the literature (Table 2). The relationships in the basin are more poorly correlated than the shelf trends ($r_{\rm nonlithogenic}^2 = 0.42$, p < .001; $r_{\rm labile}^2 = 0.15$, p < .001; Fig. 9D). We suspect this is due to the low concentrations of non-lithogenic and labile pFe observed in the basins. We note that slope stations add scatter to the basin and slope trends, which may be due to unique conditions at each slope station, such as surface sea ice melt (at marginal ice zone stations 8 and 10) or resuspension along the shelf break.

Vanadium may also be adsorbed by Mn oxyhydroxides. Thus, we also considered the relationship of labile and non-lithogenic pV to pMn fractions. Our analyses suggest that pMn-V interactions might be important in the basins where pFe concentrations are often lower than pMn concentrations. We examined the pV and pMn relationship in property-property space using the non-lithogenic and labile fractions (Figs. 9E, F). Shelf-only and slope-only trends show strong correlations in the labile fraction; the shelf samples have a steep slope and basin samples have a comparatively lower slope (shelf: $r_{labile}^2 = 0.70$, p < .001; basin: r_{labile}^2 = 0.81, p < .001). On the shelf, the pV:pMn correlation might not be causative; the increasing pV is likely driven by the much larger pFe concentrations, as discussed above. The trends in both the shelf and the basin are weaker for the non-lithogenic fractions (shelf: $r_{\text{nonlithogenic}}^2 = 0.27$, p = .006; basin: $r_{\text{nonlithogenic}}^2 = 0.56$, p < .001). Possible explanations for the differences in labile and nonlithogenic data were discussed in Section 2.5. For the basin samples, where pMn is generally greater than pFe, we tentatively interpret the pV:pMn slopes as representative of an adsorptive pV:pMn relationship.

Interestingly, the slopes derived from our labile and non-lithogenic basin pV:pMn observations are 30-40 times greater than the relationship reported in Bauer et al. (2017) (Table 2). This may suggest that our data are only correlative, and that pV may not be driven by pMn. However, in the Baltic Sea environment studied by Bauer et al. (2017) pMn concentrations can be much higher than those in our Arctic section and dV is significantly lower than in the Arctic water column. Bauer et al. (2017) described the relationship between pV and pMn in an environment where Mn is effectively trapped at the oxic-anoxic interface in the water column, whereas the relationships we observed in the Arctic Ocean are defined in an oxic water column. In the suboxic zone of the Black Sea, Yiğiterhan et al. (2011) observed similar non-lithogenic pV/pMn ratios as Bauer et al. (2017) but could not resolve whether the Mn or Fe oxyhydroxides were the controlling phase. Thus, the different pV:pMn ratios in the Baltic and Black Seas versus the Arctic Ocean are not unreasonable. We thereby chose to assess our system using the stoichiometry observed in our system; further investigation would be required to determine the reasons for the large difference in pV:pMn stoichiometry between studies.

We calculated the $pV_{CHEM,Mn}$ by multiplying labile or non-lithogenic pMn with our V:Mn ratio (Table 2). The distribution of percent $pV_{CHEM,Mn}$ indicates that the abundance of pMn in the basins, away from the continental slopes could be responsible for a significant portion of the basin pV distribution (Fig. 8G, H; see also Fig. S5B for full depth sections). However, on the shelf and slope, $pV_{CHEM,Mn}$ is far less

important, which is in agreement with the greater amount of pFe than pMn in the shelf/slope environment and our analysis above of pV_{CHEM} ,

Overall, the tight correlation between pFe and pV in our data is evidence that the distribution of pV, and thus dV, is largely influenced by scavenging of V to Fe oxides. This relationship predominates on the shelves where pFe concentrations are highest and are also much greater than pMn concentrations. In contrast, the relationship between pV and pMn in the basins and the distribution of percent pV_{CHEM,Mn} indicates that pMn may assume a more dominant role on the pV cycle in those waters where pMn is greater than pFe. Notably, because particle concentrations in the basins are so much lower than on the shelves, the relative influence of particle scavenging on dV in the basins is also much less, resulting in a largely conservative dV distribution in shallow basin waters (Section 5.1).

4.2.4. Reducing shelf environment

The final mechanism for dV removal is reduction at the sedimentwater interface or within shelf sediments (Joung and Shiller, 2016; Scholz et al., 2011; Shiller and Mao, 1999). Under reducing conditions, V(V) is reduced to V(IV) and sometimes V(III). V(IV) and V(III) species tend to rapidly partition to solid phases (Huang et al., 2015; Wehrli and Stumm, 1989). Given the previously described particle associations between V and Fe or Mn oxyhydroxides (Section 4.2.3), particle-bound V delivered to the sediments has the potential to be further immobilized in the sediments (Scholz et al., 2017; Scholz et al., 2011). Scholz et al. (2011) indicate that the formation of authigenic V in sediments requires highly reducing sediments. Indeed, analysis of various continental margin sediments suggests that V only becomes enriched in sediments under strongly reducing conditions such as where an oxygen deficient zone impinges on the bottom and Fe reduction occurs at the sedimentwater interface (Morford and Emerson, 1999). Where there was slight oxygen penetration into the sediments (< 1 cm), Morford and Emerson (1999) found release of V from margin sediments. V depletion has been observed in hypoxic waters of the Louisiana Shelf (Joung and Shiller, 2016; Shiller and Mao, 1999) and seasonally variable V depletion and enrichment was reported for waters in the Mississippi Sound and Bight where hypoxia is less extensive (Ho et al., 2019).

Hardison et al. (2017) reported only slight oxygen penetration (5–8 mm) in sediments from the north-eastern Chukchi Sea and Brüchert et al. (2018) found similarly slight oxygen penetration in sediments of the East Siberian Shelf. Anderson et al. (2017) suggested that nitrate depletion (relative to phosphate) in the East Siberian Sea was indicative of hypoxia. Additionally, Kvitek et al. (1998) note the possibility of anoxic brine filled ice gouges in an Arctic embayment. Thus, while sediments were not examined as a part of this study, it is reasonable to expect conditions favorable for immobilization of V on some Arctic shelves.

From the GN01 section, there are further indicators that the shelf sediments are reducing enough to remove dV and that sediment-water exchange may be a V sink on the shelf. For example, under the reducing conditions wherein dV can be removed from solution, pMn is released to the dissolved phase (Wang and Sañudo-Wilhelmy, 2008). High dMn concentrations at GN01 shelf stations indicate that the shelf is a source of dMn (Jensen et al., 2018; Shiller, 2019) and, thus, also likely a sink for V. Kondo et al. (2016) also observed elevated dMn in bottom waters of the outer shelf, which indicates consistency between years and across the spatial area of the Chukchi Shelf. Additionally, dissolved methane was elevated in some shelf bottom waters during the GN01 cruise (Whitmore and Shiller, 2016), indicating a sediment source of dissolved methane (although several other methane sources are possible). The δ¹³C signature of methane in samples collected from the Bering and Chukchi shelves in 2012 was indicative of a microbial source (Kudo et al., 2018) which implies highly reducing shelf sediment conditions. Thus, while we cannot quantitatively ascribe sediment reduction as a dV removal mechanism, it is likely that reducing shelf conditions play

an important role in removing dV from Arctic shelf waters.

Off the Peru margin, Ho et al. (2018) did not observe the sort of shelf influence we see in the Arctic, despite the operation of an Fe shuttling mechanism there (Scholz et al., 2011). The reason for this difference is probably physiographic: as noted in our introduction, shelves comprise half the area of the Arctic Ocean; in contrast, the Peru margin is narrow, especially when compared to the expanse of the Pacific Ocean.

4.2.5. The Arctic Ocean V cycle

In this consideration of mechanisms responsible for dV removal, we demonstrated that mixing of endmembers does not account for low dV observed in the waters of the basins. Biology likely has a significant role in near surface waters, but a minor role below that; even on the shelves, pV_{BIO} accounts for little of the labile pV below the very surface. However, pFe, which is elevated on the shelves, does have a strong relationship with pV, suggesting that Fe oxides exert a control on the V cycle. Particulate V trended significantly with pMn only in the basins where pFe was very low. The large amount of particles on the shelf compared to the basins suggests the role of the shelf in setting basin geochemistry is substantial.

We suggest the same paired sorption-reduction mechanism that Scholz et al. (2011, 2017) described for V removal in the Peruvian margin is occurring over the Bering and Chukchi shelves and likely other Arctic shelves. Delivery of V to shelf sediments in our region is likely driven by V scavenged by authigenic marine oxides (predominantly Fe oxides) and to a minor degree by biologically-associated V. Particulate V may subsequently be immobilized within the shelf sediments due to its reduction to less soluble forms. Low dV shelf-influenced waters are advected into the central Arctic basins, whereby a surface depletion is observed. If our suggested mechanism is correct, the extensive shelf V removal might make the Arctic Ocean one place where water column V isotope fraction (Wu et al., 2019) could be observed.

Shiller and Mao (1999) suggested that expansion of anthropogenic shelf hypoxia might increase the shelf contribution to dV removal from seawater. Importantly, our Arctic Ocean data suggest that shelf removal of dV could be a non-trivial aspect of the V cycle, especially in marginal seas with large shelf regions. Furthermore, if climate change factors such as declining sea ice contribute to changing biogeochemical cycling in the Arctic (e.g., Anderson et al., 2017), then the Arctic Ocean dV distribution may be an indicator of the impact of that change.

4.3. Deep water dV distribution

The deep and bottom water dV concentrations we observed in the Arctic Ocean (dV = 30.1 ± 0.9 where z > $2000 \, \text{m}$) are lower than reports from other deep ocean basins (Collier, 1984; Ho et al., 2018; Middelburg et al., 1988). There are only a few mechanisms by which Arctic Deep Water (ADW) could have diminished dV relative to other ocean basins: source waters of ADW could have low dV to begin with; the source waters could be modified during their transformation into ADW; or, there could be slow removal of dV during the long residence time of ADW. Since the deep waters of each basin we sampled (Makarov, Canada, and Eurasian) have the same dV concentration, despite having different apparent ages (e.g., Schlosser et al., 1997), slow removal of dV is unlikely to be a significant factor. Supporting this is the observation that in the global ocean deep water dV only slightly increases between the Atlantic and Pacific Ocean (Ho et al., 2018; Middelburg et al., 1988); therefore, slow scavenging removal is unlikely a major factor in the dV distribution.

Jones et al. (1995) indicate three main sources of Arctic Deep Water: a) continental slope density flows comprised mainly of Atlantic and intermediate layer waters but triggered by shelf brines, b) Barents Sea Branch Waters (BSBW), and c) Fram Strait Branch Waters (FSBW). They suggest that the density flows are the most important component

while FSBW is the least important component. Regardless of the relative magnitudes of these sources, it would seem that, except for FSBW, the sources of ADW have experienced substantial shelf interactions and thus likely would have diminished dV relative to their external source, such as we observed in the TPD and elsewhere in shallow Arctic waters.

With regard to the external source of ADW, most of this is from the North Atlantic which, as noted previously, enters the Arctic Ocean via the Fram Strait and the Barents Sea, having sill depths of roughly 2500 m and 200 m, respectively (Rudels, 2019; von Appen et al., 2015). In shallow North Atlantic waters, Klein et al. (2013) observed a range of surface dV in the North Atlantic of 12–32 nmol/kg (5–10 m water depth) and Middelburg et al. (1988) observed surface dV of 31.7–35.2 nmol/kg (< 100 m depth). Because of the sill depths we should also consider deeper waters that enter the Arctic, which according to Middelburg et al. (1988) are roughly 32.5 nmol/kg.

It thus seems likely that ADW has diminished dV due partly to the slightly low dV of inflowing shallow North Atlantic waters but also due to additional removal of dV as these waters interact with the shelves. To better assess the ADW dV signature, dissolved V data from the Eurasian side of the Arctic would be required to further characterize deep water distributions and assess endmember values.

4.4. Utility as a tracer

Geochemical tracers can be used to inform us about the mechanisms driving water mass modifications on the shelves and the connectivity between the shelf and the basin. Additionally, because Arctic waters are a key driver of global circulation processes, understanding geochemical distributions in the Arctic marine system can help us further utilize the distributions of trace elements and their isotopes globally.

One of the most prominent features in the western Arctic Basins is the Pacific halocline, formed from a mixture of lower-salinity sources such as sea ice melt, river drainage, and Pacific water. Pacific halocline waters are often traced with a combined nutrient tracer, which is only quasi-conservative, in part due to the non-conservative behavior of the nutrients (e.g., Alkire et al., 2015; Newton et al., 2013). Although there are concerns with the quantitative results of the nutrient tracer, there are few other tracers that have been described that can deconvolve these water masses. Thus, there is a demand for tracers that can elucidate the Arctic marine system more clearly. Our V data reveal a distribution wherein in the Pacific halocline has less dV than Atlantic waters below and less than Pacific waters entering the Arctic. This distribution reveals the extent of shelf modification on Arctic water masses from the incoming Pacific and Atlantic waters.

We note that interactions of V with particles predominantly influence dV on the shelves, but Fe and Mn oxyhydroxides have the potential to alter dV distribution in the basins. To assess if our basin distribution behaves conservatively, as is often the case with dV in oceanic waters below the euphotic zone (e.g., Morris, 1975), we examined the dV associated with each water mass as a function of location in the basin. In this case, distance from the margin is a rough proxy for age (i.e., exposure to potential non-conservative processes) (Fig. 10).

Using average dV for each water mass at each station, we determined that dV in the polar mixed layer, the Atlantic halocline, and Arctic deep waters basin did not significantly change with distance from the shelf (Fig. 10). We note that the Pacific halocline dV had a poor correlation with latitude ($\mathbf{r}^2=0.37; p=.05$). However, the normalized dV_{saline} showed a stronger correlation ($\mathbf{r}^2=0.57; p=.01$) (Table S3; Fig. S6). In the Makarov Basin and Canada Basin we used data between 75°N and 85°N and data between 73°N and 85°N, respectively (i.e., the shelf break and the northern-most limit of the Pacific halocline). These correlations suggest that, in general, behavior of dV in the basins is conservative. However, in the Pacific halocline there may be some non-conservative behavior.

Our data lend support to interactions with reducing environments and scavenging by Fe-oxyhydroxides as primary drivers for V removal

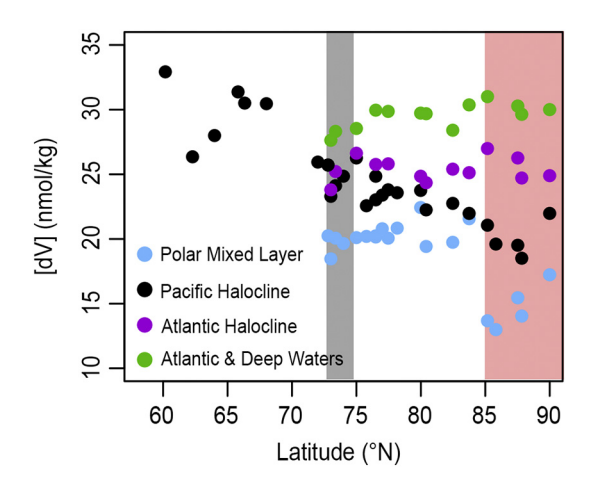


Fig. 10. Dissolved V versus latitude. Dissolved V (nmol/kg) in the GN01 Section, dV concentrations presented are averages at each station for the respective water masses. The gray shaded region represents the shelf break and the red shaded region represents stations north of the pacific halocline (which also have TPD-influenced surface waters). (For interpretation of the references to color in this figure legend, the reader is referred to the web version of this article.)

on the shelves. While the conditions that impart depleted dV signals are highly dynamic and may not be conducive to separating endmembers, it appears that dV falls into a suite of tools that can help unify our understanding of the Arctic marine system.

5. Conclusions

In the western Arctic Ocean basins, the vertical distribution of dissolved vanadium (dV) shows a surface depletion of 24-49% with respect to deep water dV. The depleted surface waters are associated with water mass features (i.e., the Pacific halocline, Polar Mixed Layer, and Transpolar Drift), which indicates that lateral transport from shelf waters is important in setting the dV signature in the basins. A consideration of processes that could influence the dV distribution suggests that scavenging of V by Fe oxyhydroxides and delivery to the sediments is the dominant mechanism by which V is removed from the water column. To a minor degree, biological removal in the surface layer and scavenging associated with Mn oxyhydroxides may also contribute to the water column removal of dV. The dV depletion is likely facilitated by an Fe shuttling mechanism (Scholz et al., 2011, 2017) whereby Fe oxyhydroxides delivered to Arctic shelf sediments are reductively dissolved in the sediments. The dissolved Fe diffusing from the sediments is ultimately re-oxidized and precipitated in the oxic shelf water column and thus further removes dV by repeating the scavenging process. Evidence suggests that the shelf sediments are likely reducing enough to reduce and immobilize the shuttled V within them. Vanadium-depleted shelf waters are subsequently advected into the basins, where dV behaves roughly conservatively.

Deep basin waters in the Western Arctic Ocean are significantly lower in dV concentration than other ocean basins. This may be indicative of sources of water to the deep basin and further study is needed to determine the extent to which the depletion results from direct endmember contributions or substantial margin influence on incoming deep Arctic source waters.

Further studies of V in the water column and sediments of the Arctic basin and on the regional continental shelves will help better constrain the processes, influence, and extent of shelf modification on the basin dV signature. Arctic Ocean waters leave the Arctic predominantly via the Fram and Davis Straits and contribute to formation of intermediate and deep waters in the North Atlantic. The study of tracers in these water masses must include the Arctic as an important site of modification to tracer signals. Our Arctic work also raises important

questions as to the net effect of marginal basin shelves on oceanic vanadium cycling, its isotopic balance, and how climate-induced changes in shelf biogeochemical cycling will impact vanadium cycling.

Declaration of Competing Interest

None.

Acknowledgements

This research was supported by the National Science Foundation [OCE-1436312 (AMS), OCE-1435862 (BST), OCE-1436019 (PLM)]. We extend thanks to Melissa Gilbert for her analytical ICP-MS work at the University of Southern Mississippi's Center for Trace Analysis and Angelique White for the pigment analyses. We also thank the USCGC Healy's crew and the scientific leadership, Bill Landing, Greg Cutter, and Dave Kadko, for their support of a successful expedition. The manuscript was improved by comments from Bill Landing and two anonymous reviewers.

Appendix A. Supplementary data

Supplementary data to this article can be found online at https://doi.org/10.1016/j.marchem.2019.103701.

References

Aagaard, K., 1981. On the deep circulation in the Arctic Ocean. Deep Sea Res. 251–268 28A.

Aguilar-Islas, A.M., Rember, R., Nishino, S., Kikuchi, T., Itoh, M., 2013. Partitioning and lateral transport of iron to the Canada Basin. Polar Sci. 7, 82–99. https://doi.org/10.1016/j.polar.2012.11.001.

Alkire, M.B., Morison, J., Andersen, R., 2015. Variability in the meteoric water, sea-ice melt, and Pacific water contributions to the Central Arctic Ocean, 2000-2014. J. Geophys. Res. Oceans 120, 1573–1598. https://doi.org/10.1002/2014JC010023.

Anderson, L.G., Björk, G., Holby, O., Jutterström, S., Mörth, C.M., O&apos, Regan, M., Pearce, C., Semiletov, I., Stranne, C., Stöven, T., Tanhua, T., Ulfsbo, A., Jakobsson, M., 2017. Shelf–Basin interaction along the East Siberian Sea. Ocean Sci. 13, 349–363. https://doi.org/10.5194/os-13-349-2017.

Bauch, D., Schlosser, P., Fairbanks, R., 1995. Freshwater balance and the sources of deep and bottom waters in the Arctic Ocean inferred from the distribution of H₂¹⁸O. Prog. Oceanogr. 35, 53–80.

Bauer, S., Blomqvist, S., Ingri, J., 2017. Distribution of dissolved and suspended particulate molybdenum, vanadium, and tungsten in the Baltic Sea. Mar. Chem. 196, 135–147. https://doi.org/10.1016/j.marchem.2017.08.010.

Beck, A.J., Cochran, J.K., Sañudo-Wilhelmy, S.A., 2010. The distribution and speciation of dissolved trace metals in a shallow subterranean estuary. Mar. Chem. 121, 145–156. https://doi.org/10.1016/j.marchem.2010.04.003.

Berger, C.J.M., Lippiatt, S.M., Lawrence, M.G., Bruland, K.W., 2008. Application of a chemical leach technique for estimating labile particulate aluminum, iron, and manganese in the Columbia River plume and coastal waters off Oregon and Washington. J. Geophys. Res. 113, C00B01. https://doi.org/10.1029/2007.10004703

Blais, M., Tremblay, J.-É., Jungblut, A.D., Gagnon, J., Martin, J., Thaler, M., Lovejoy, C., 2012. Nitrogen fixation and identification of potential diazotrophs in the Canadian Arctic: N₂ fixation in the Arctic Ocean. Glob. Biogeochem. Cycles 26. https://doi.org/ 10.1029/2011GB004096.

Breit, G.N., Wanty, R.B., 1991. Vanadium accumulation in carbonaceous rocks: a review of geochemical controls during deposition and diagenesis. Chem. Geol. 91, 83–97. https://doi.org/10.1016/0009-2541(91)90083-4.

Brinza, L., Benning, L.G., Statham, P.J., 2008. Adsorption studies of Mo and V onto ferrihydrite. Mineral. Mag. 72, 385–388. https://doi.org/10.1180/minmag.2008.072.1.

Brüchert, V., Bröder, L., Sawicka, J.E., Tesi, T., Joye, S.P., Sun, X., Semiletov, I.P., Samarkin, V.A., 2018. Carbon mineralization in Laptev and east Siberian sea shelf and slope sediment. Biogeosciences 15, 471–490. https://doi.org/10.5194/bg-15-471.2018

Charette, M.A., Lam, P.J., Lohan, M.C., Kwon, E.Y., Hatje, V., Jeandel, C., Shiller, A.M., Cutter, G.A., Thomas, A., Boyd, P.W., Homoky, W.B., Milne, A., Thomas, H., Andersson, P.S., Porcelli, D., Tanaka, T., Geibert, W., Dehairs, F., Garcia-Orellana, J., 2016. Coastal ocean and shelf-sea biogeochemical cycling of trace elements and isotopes: lessons learned from GEOTRACES. Philos. Trans. R. Soc. Math. Phys. Eng. Sci. 374, 20160076. https://doi.org/10.1098/rsta.2016.0076.

Cid, A.P., Nakatsuka, S., Sohrin, Y., 2012. Stoichiometry among bioactive trace metals in the Chukchi and Beaufort seas. J. Oceanogr. 68, 985–1001. https://doi.org/10.1007/ s10872-012-0150-8.

Collier, R.W., 1984. Particulate and dissolved vanadium in the North Pacific Ocean.

- Nature 390, 441-444.
- Crans, D.C., Smee, J.J., Gaidamauskas, E., Yang, L., 2004. The chemistry and biochemistry of vanadium and the biological activities exerted by vanadium compounds. Chem. Rev. 104, 849–902.
- Cutter, G., Andersson, P.S., Codispoti, L.A., Croot, P., Francois, R., Lohan, M., Obata, Hajime, Rutgers van der Loeff, M., 2014. Sampling and Sample-Handling Protocols for GEOTRACES Cruises Version 2. http://www.geotraces.org/library-88/scientific-publications/reports/169-sampling-and-sample-handling-protocols-for-geotraces-cruises
- Cutter, G., Kadko, D., Landing, W., 2019a. Bottle data from the CTD-ODF carousel on the GEOTRACES Arctic Section cruise (HLY1502) from August to October 2015 (U.S. GEOTRACES Arctic project). Biol. Chem. Oceanogr. Data Manag. Off. (BCO-DMO). https://doi.org/10.1575/1912/bco-dmo.646825.4. Dataset version 2019-07-29.
- Cutter, G., Kadko, D., Landing, W., 2019b. Bottle data from the GEOTRACES Clean Carousel sampling system (GTC) on the Arctic Section cruise (HLY1502) from August to October 2015 (U.S. GEOTRACES Arctic project). Biol. Chem. Oceanogr. Data Manag. Off. (BCO-DMO). https://doi.org/10.1575/1912/bco-dmo.647259.4. Dataset version 2019-07-29.
- Emerson, S.R., Huested, S.S., 1991. Ocean anoxia and the concentrations of molybdenum and vanadium in seawater. Mar. Chem. 34, 177–196. https://doi.org/10.1016/0304-4203(91)90002-E.
- Feely, R.A., Tefry, J.H., Lebon, G.T., German, C.R., 1998. The relationship between P/Fe adn V/Fe ratios in hydrothermal precipitates and dissolved phosphate in seawater. Geophys. Res. Lett. 25 (13), 2253–2256. https://doi.org/10.1029/98GL01546.
- Fernández-Méndez, M., Turk-Kubo, K.A., Buttigieg, P.L., Rapp, J.Z., Krumpen, T., Zehr, J.P., Boetius, A., 2016. Diazotroph diversity in the sea ice, melt ponds, and surface waters of the Eurasian Basin of the Central Arctic Ocean. Front. Microbiol. 7, 1884. https://doi.org/10.3389/fmicb.2016.01884.
- Fransson, A., Chierici, M., Anderson, L.G., Bussmann, I., Kattner, G., Peter Jones, E., Swift, J.H., 2001. The importance of shelf processes for the modification of chemical constituents in the waters of the Eurasian Arctic Ocean: implication for carbon fluxes. Cont. Shelf Res. 21, 225–242. https://doi.org/10.1016/S0278-4343(00)00088-1.
- Harding, K., Turk-Kubo, K.A., Sipler, R.E., Mills, M.M., Bronk, D.A., Zehr, J.P., 2018. Symbiotic unicellular cyanobacteria fix nitrogen in the Arctic Ocean. Proc. Natl. Acad. Sci. 115, 13371–13375. https://doi.org/10.1073/pnas.1813658115.
- Hardison, A.K., McTigue, N.D., Gardner, W.S., Dunton, K.H., 2017. Arctic shelves as platforms for biogeochemical activity: nitrogen and carbon tranformations in the Chukchi Sea, Alaska. Deep Sea Research Part II: Topical Studies in Oceanography 144, 78–91. https://doi.org/10.1016/j.dsr2.2017.08.004.
- Ho, P., Lee, J.-M., Heller, M.I., Lam, P.J., Shiller, A.M., 2018. The distribution of dissolved and particulate Mo and V along the U.S. GEOTRACES East Pacific Zonal transect (GP16): the roles of oxides and biogenic particles in their distributions in the oxygen deficient zone and the hydrothermal plume. Mar. Chem. 201, 242–255. https://doi. org/10.1016/j.marchem.2017.12.003.
- Ho, P., Shim, M.J., Howden, S.D., Shiller, A.M., 2019. Temporal and spatial distributions of nutrients and trace elements (Ba, Cs, Cr, Fe, Mn, Mo, U, V and re) in Mississippi coastal waters: influence of hypoxia, submarine groundwater discharge, and episodic events. Cont. Shelf Res. 175. 53–69. https://doi.org/10.1016/j.csr.2019.01.013.
- Honjo, S., Krishfield, R.A., Eglinton, T.I., Manganini, S.J., Kemp, J.N., Doherty, K., Hwang, J., McKee, T.K., Takizawa, T., 2010. Biological pump processes in the cryopelagic and hemipelagic Arctic Ocean: Canada Basin and Chukchi rise. Prog. Oceanogr. 85, 137–170. https://doi.org/10.1016/j.pocean.2010.02.009.
- Huang, J.-H., Huang, F., Evans, L., Glasauer, S., 2015. Vanadium: global (bio)geochemistry. Chem. Geol. 417, 68–89. https://doi.org/10.1016/j.chemgeo.2015.09.019.
- Jakobsson, M., 2002. Hypsometry and volume of the Arctic Ocean and its constituent seas. Geochem. Geophys. Geosystems 3, 1–18. https://doi.org/10.1029/ 2001GC000302.
- Jeandel, C., Peucker-Ehrenbrink, B., Jones, M.T., Pearce, C.R., Oelkers, E.H., Godderis, Y., Lacan, F., Aumont, O., Arsouze, T., 2011. Ocean margins: the missing term in oceanic element budgets? EOS Trans. Am. Geophys. Union 92, 217–224. https://doi.org/10. 1029/2011E0260001.
- Jensen, L., Cullen, J.T., Ball, G.T., Sherrell, R.M., Fitzsimmons, J.N., 2018. CT13A-04: Dissolved Fe and Mn along US Arctic GEOTRACES GN01: Effects of Scavenging in Intermediate and Deep Waters.
- Jones, E.P., Rudels, B., Anderson, L.G., 1995. Deep waters of the Arctic Ocean: origins and circulation. Deep Sea Res. Part Oceanogr. Res. Pap. 42, 737–760. https://doi.org/10. 1016/0967-0637(95)00013-V.
- Joung, D., Shiller, A.M., 2016. Temporal and spatial variations of dissolved and colloidal trace elements in Louisiana shelf waters. Mar. Chem. 181, 25–43. https://doi.org/10. 1016/j.marchem.2016.03.003.
- Kipp, L.E., Charette, M.A., Moore, W.S., Henderson, P.B., Rigor, I.G., 2018. Increased fluxes of shelf-derived materials to the central Arctic Ocean. Sci. Adv. 4, eaao1302. https://doi.org/10.1126/sciadv.aao1302.
- Klein, N.J., Beck, A.J., Hutchins, D.A., Sañudo-Wilhelmy, S.A., 2013. Regression modeling of the North East Atlantic Spring Bloom suggests previously unrecognized biological roles for V and Mo. Front. Microbiol. 4, 45. https://doi.org/10.3389/fmicb.2013.00045.
- Klunder, M.B., Laan, P., Middag, R., de Baar, H.J.W., Bakker, K., 2012. Dissolved iron in the Arctic Ocean: important role of hydrothermal sources, shelf input and scavenging removal: Dissoved iron in the Arctic Ocean. J. Geophys. Res. Oceans 117, C04014. https://doi.org/10.1029/2011JC007135.
- Knauer, G.A., Martin, J.H., 1981. Phosphorus-cadmium cycling in northeast Pacific waters. J. Mar. Res. 39 (1), 65–76.
- Kondo, Y., Obata, Hajime, Hioki, N., Ooki, A., Nishino, S., Kikuchi, T., Kuma, K., 2016. Transport of trace metals (Mn, Fe, Ni, Zn and Cd) in the western Arctic Ocean (Chukchi Sea and Canada Basin) in late summer 2012. Deep Sea Res. Part Oceanogr.

- Res. Pap. 116, 236-252. https://doi.org/10.1016/j.dsr.2016.08.010.
- Koschinsky, A., Hein, J.R., 2003. Uptake of elements from seawater by ferromanganese crusts: solid-phase associations and seawater speciation. Mar. Geol. 198, 331–351. https://doi.org/10.1016/S0025-3227(03)00122-1.
- Kudo, K., Yamada, K., Toyoda, S., Yoshida, N., Sasano, D., Kosugi, N., Ishii, M., Yoshikawa, H., Murata, A., Uchida, H., Nishino, S., 2018. Spatial distribution of dissolved methane and its source in the western Arctic Ocean. J. Oceanogr. 74, 305–317. https://doi.org/10.1007/s10872-017-0460-y.
- Kvitek, R.G., Conlan, K.E., lampietro, P.J., 1998. Black pools of death: hypoxic, brine-filled ice gouge depressions become lethal traps for benthic organisms in a shallow Arctic embayment. Mar. Ecol. Prog. Ser. 162, 1–10. https://doi.org/10.3354/meps162001.
- Macdonald, R.W., Gobeil, C., 2012. Manganese sources and sinks in the Arctic Ocean with reference to periodic enrichments in basin sediments. Aquat. Geochem. 18, 565–591. https://doi.org/10.1007/s10498-011-9149-9.
- Marsay, C.M., Aguilar-Islas, A., Fitzsimmons, J.N., Hatta, M., Jensen, L.T., John, S.G., Kadko, D., Landing, W.M., Lanning, N.T., Morton, P.L., Pasqualini, A., Rauschenberg, S., Sherrell, R.M., Shiller, A.M., Twining, B.S., Whitmore, L.M., Zhang, R., Buck, C.S., 2018. Dissolved and particulate trace elements in late summer Arctic melt ponds. Mar. Chem. 204, 70–85. https://doi.org/10.1016/j.marchem.2018.06.002.
- Mauldin, A., Schlosser, P., Newton, R., Smethie, W.M., Bayer, R., Rhein, M., Jones, E.P., 2010. The velocity and mixing time scale of the Arctic Ocean boundary current estimated with transient tracers. J. Geophys. Res. 115, C08002. https://doi.org/10. 1029/2009JC005965.
- Middag, R., de Baar, H.J.W., Laan, P., Bakker, K., 2009. Dissolved aluminium and the silicon cycle in the Arctic Ocean. Mar. Chem. 115, 176–195. https://doi.org/10. 1016/j.marchem.2009.08.002.
- Middelburg, J.J., Hoede, D., Van Der Sloot, H.A., Van Der Weijden, C.H., Wijkstra, J., 1988. Arsenic, antimony and vanadium in the North Atlantic Ocean. Geochim. Cosmochim. Acta 52, 2871–2878. https://doi.org/10.1016/0016-7037(88)90154-8.
- Morford, J.L., Emerson, S., 1999. The geochemistry of redox sensitive trace metals in sediments. Geochim. Cosmochim. Acta 63, 1735–1750. https://doi.org/10.1016/ S0016-7037(99)00126-X.
- Morris, A.W., 1975. Dissolved molybdenum and vanadium in the northeast Atlantic Ocean. Deep Sea Res. Oceanogr. Abstr. 22, 49–54. https://doi.org/10.1016/0011-7471(75)90018-2.
- Newton, R., Schlosser, P., Mortlock, R., Swift, J., MacDonald, R., 2013. Canadian Basin freshwater sources and changes: results from the 2005 Arctic Ocean section: AOS 2005 freshwater sources and changes. J. Geophys. Res. Oceans 118, 2133–2154. https://doi.org/10.1002/jgrc.20101.
- Nuester, J., Vogt, S., Newville, M., Kustka, A.B., Twining, B.S., 2012. The unique biogeochemical signature of the marine Diazotroph Trichodesmium. Front. Microbiol. 3, 150. https://doi.org/10.3389/fmicb.2012.00150.
- O'Brien, M.C., Melling, H., Pedersen, T.F., Macdonald, R.W., 2013. The role of eddies on particle flux in the Canada Basin of the Arctic Ocean. Deep Sea Res. Part Oceanogr. Res. Pap. 71, 1–20. https://doi.org/10.1016/j.dsr.2012.10.004.
- Ohnemus, D.C., Lam, P.J., 2015. Cycling of lithogenic marine particles in the US GEOTRACES North Atlantic transect. Deep Sea Res. Part II Top. Stud. Oceanogr. 116, 283–302. https://doi.org/10.1016/j.dsr2.2014.11.019.
- Ohnemus, D.C., Auro, M.E., Sherrell, R.M., Lagerström, M., Morton, P.L., Twining, B.S., Rauschenberg, S., Lam, P.J., 2014. Laboratory intercomparison of marine particulate digestions including piranha: a novel chemical method for dissolution of polyethersulfone filters. Limnol. Oceanogr. Methods 12, 530–547. https://doi.org/10. 4319/Jonr.2014.12.530
- Ohnemus, D.C., Rauschenberg, S., Cutter, G.A., Fitzsimmons, J.N., Sherrell, R.M., Twining, B.S., 2017. Elevated trace metal content of prokaryotic communities associated with marine oxygen deficient zones: elevated trace metals in ODZ prokaryotes. Limnol. Oceanogr. 62, 3–25. https://doi.org/10.1002/lno.10363.
- Osterholz, H., Simon, H., Beck, M., Maerz, J., Rackebrandt, S., Brumsack, H.-J., Feudel, U., Simon, M., 2014. Impact of diatom growth on trace metal dynamics (Mn, Mo, V, U). J. Sea Res. 87, 35–45. https://doi.org/10.1016/j.seares.2013.09.009.
- Peterson, B.J., Holmes, R.M., McClelland, J.W., Amon, R., Brabets, T., et al., 2016.
 PARTNERS Project Arctic River Biogeochemical Data. Arct. Data Cent. https://doi.org/10.18739/A2166T.
- Proshutinsky, A.Y., Johnson, M.A., 1997. Two circulation regimes of the wind-driven Arctic Ocean. J. Geophys. Res. Oceans 102, 12493–12514. https://doi.org/10.1029/97JC00738
- Reckhardt, A., Beck, M., Greskowiak, J., Schnetger, B., Böttcher, M.E., Gehre, M., Brumsack, H.-J., 2017. Cycling of redox-sensitive elements in a sandy subterranean estuary of the southern North Sea. Mar. Chem. 188, 6–17. https://doi.org/10.1016/j. marchem.2016.11.003.
- Roeske, T., Rutgers van der Loeff, M., Middag, R., Bakker, K., 2012. Deep water circulation and composition in the Arctic Ocean by dissolved barium, aluminium and silicate. Mar. Chem. 132–133, 56–67. https://doi.org/10.1016/j.marchem.2012.02.001.
- Rudels, B., 2019. Arctic Ocean circulation. In: Encyclopedia of Ocean Sciences. Elsevier, pp. 262–277. https://doi.org/10.1016/B978-0-12-409548-9.11209-6.
- Rudels, B., Quadfasel, D., 1991. Convection and deep water formation in the Arctic Ocean-Greenland Sea system. J. Mar. Syst. 2, 435–450. https://doi.org/10.1016/ 0924-7963(91)90045-V.
- Rudnick, R.L., Gao, S., 2014. 4.1 composition of the continental crust. In: Treatise on Geochemistry. Elsevier, Oxford, pp. 1–51.
- Schlitzer, R., 2018. Ocean Data View 5.1.5. [WWW Document]. URL. https://odv.awi.de. Schlosser, P., Kromer, B., Ekwurzel, B., Bönisch, G., McNichol, A., Schneider, R., von Reden, K., Östlund, H.G., Swift, J.H., 1997. The first trans-Arctic 14C section: comparison of the mean ages of the deep waters in the Eurasian and Canadian basins of

the Arctic Ocean. Nucl. Instrum. Methods Phys. Res. Sect. B Beam Interact. Mater. At. 123, 431–437. https://doi.org/10.1016/S0168-583X(96)00677-5.

- Scholz, F., Hensen, C., Noffke, A., Rohde, A., Liebetrau, V., Wallmann, K., 2011. Early diagenesis of redox-sensitive trace metals in the Peru upwelling area response to ENSO-related oxygen fluctuations in the water column. Geochim. Cosmochim. Acta 75, 7257–7276. https://doi.org/10.1016/j.gca.2011.08.007.
- Scholz, F., Siebert, C., Dale, A.W., Frank, M., 2017. Intense molybdenum accumulation in sediments underneath a nitrogenous water column and implications for the reconstruction of paleo-redox conditions based on molybdenum isotopes. Geochim. Cosmochim. Acta 213, 400–417. https://doi.org/10.1016/j.gca.2017.06.048.
- Shiller, A., 2019. Dissolved Ba, Cd, Cu, Ga, Mn, Ni, and V concentration data from the US GEOTRACES Arctic Expeditions (GN01, HLY1502) from August to October 2015. In: Biol. Chem. Oceanogr. Data Manag. Off. BCO-DMO Dataset version 2019-07-09, https://doi.org/10.1575/1912/bco-dmo.772645.1.
- Shiller, A.M., Mao, L., 1999. Dissolved vanadium on the Louisiana shelf: effect of oxygen depletion. Cont. Shelf Res. 1007–1020.
- Sipler, R.E., Gong, D., Baer, S.E., Sanderson, M.P., Roberts, Q.N., Mulholland, M.R., Bronk, D.A., 2017. Preliminary estimates of the contribution of Arctic nitrogen fixation to the global nitrogen budget: Arctic nitrogen fixation. Limnol. Oceanogr. Lett. 2, 159–166. https://doi.org/10.1002/lol2.10046.
- Smethie, W.M., Schlosser, P., Bönisch, G., Hopkins, T.S., 2000. Renewal and circulation of intermediate waters in the Canadian Basin observed on the SCICEX 96 cruise. J. Geophys. Res. Oceans 105, 1105–1121. https://doi.org/10.1029/1999JC900233.
- Steele, M., 2004. Circulation of summer Pacific halocline water in the Arctic Ocean. J. Geophys. Res. 109. https://doi.org/10.1029/2003JC002009.
- Takematsu, N., Sato, Y., Okabe, S., Nakayama, E., 1985. The partition of vanadium and molybdenum between manganese oxides and sea water. Geochim. Cosmochim. Acta 49, 2395–2399. https://doi.org/10.1016/0016-7037(85)90239-X.
- Talley, L.D., Pickard, G.L., Emery, W.J., Swift, J.H., 2011. Arctic Ocean and Nordic seas. In: Descriptive Physical Oceanography. Elsevier, pp. 401–436. https://doi.org/10. 1016/B978-0-7506-4552-2.10012-5.
- Tang, D., François, M.M., 2006. Distinguishing between cellular and Fe-oxide-associated trace elements in phytoplankton. Mar. Chem. 98 (1), 18–30. https://doi.org/10. 1016/j.marchem.2005.06.003.
- Tovar-Sanchez, A., Sañudo-Wilhelmy, S.A., 2011. Influenc of the Amazon River on

- dissolved and intracellular metal concentrations in *Trichodesmium* colonies along the western boundary of the sub-tropical North Atlantic Coean. Biogeosciences 8, 217–225. https://doi.org/10.5194/bg-8-217-2011.
- Trefry, J.H., Metz, S., 1989. Role of hydrothermal precipitates in the geochemical cycling of vanadium. Nature 342, 531–533.
- Twining, B.S., Rauschenberg, S., Morton, P.L., Ohnemus, D.C., Lam, P.J., 2015.

 Comparison of particulate trace element concentrations in the North Atlantic Ocean as determined with discrete bottle sampling and in situ pumping. Deep-Sea Res. Part II Top. Stud. Oceanogr. 116, 273–282. https://doi.org/10.1016/j.dsr2.2014.11.005.
- Twining, B., Morton, P., Salters, V., 2019. Trace element concentrations (labile and total measurements) in particles collected with GO-Flo bottles and analyzed with ICP-MS from the US GEOTRACES Arctic cruise (HLY1502; GN01) from August to October 2015a. In: Biol. Chem. Oceanogr. Data Manag. Off. BCO-DMO Dataset version 2019-07-02, https://doi.org/10.1575/1912/bco-dmo.771474.2.
- Vieira, L.H., Achterberg, E.P., Scholten, J., Beck, A.J., Liebetrau, V., Mills, M.M., Arrigo, K.R., 2019. Benthic fluxes of trace metals in the Chukchi Sea and their transport into the Arctic Ocean. Mar. Chem. 208, 43–55. https://doi.org/10.1016/j.marchem.2018. 11.001
- von Appen, W.-J., Schauer, U., Somavilla, R., Bauerfeind, E., Beszczynska-Möller, A., 2015. Exchange of warming deep waters across Fram Strait. Deep Sea Res. Part Oceanogr. Res. Pap. 103, 86–100. https://doi.org/10.1016/j.dsr.2015.06.003.
- Wang, D., Sañudo-Wilhelmy, S.A., 2008. Development of an analytical protocol for the determination of V(IV) and V(V) in seawater: application to coastal environments. Mar. Chem. 112, 72–80. https://doi.org/10.1016/j.marchem.2008.05.011.
- Wehrli, B., Stumm, W., 1989. Vanadyl in natural waters: adsorption and hydrolysis promote oxygenation. Geochim. Cosmochim. Acta 53, 69–77.
- Whitmore, L.M., Shiller, A.M., 2016. Distribution and Flux of Methane in the 2015 U.S. GEOTRACES Arctic Section. 3408 Goldschmidt Abstr.
- Wu, F., Owens, J.D., Huang, T., Sarafian, A., Huang, K.-F., Sen, I.S., Horner, T.J., Blusztajn, J., Morton, P., Nielsen, S.G., 2019. Vanadium isotope composition of seawater. Geochim. Cosmochim. Acta 244, 403–415. https://doi.org/10.1016/j.gca. 2018.10.010.
- Yiğiterhan, O., Murray, J.W., Tuğrul, S., 2011. Trace metal composition of suspended particulate matter in the water column of the Black Sea. Mar. Chem. 126, 207–228. https://doi.org/10.1016/j.marchem.2011.05.006.